DANSK BIOMEKANISK SELSKAB

Program & Abstracts

15th Annual Meeting of the Danish Society of Biomechanics

24/11/2023

Welcome & Venue

Dear Colleagues

On behalf of the board of the Danish Society of Biomechanics, Department for Materials and Production, AAU, as well as the Organizing Committee, we invite you to the 15th annual meeting on November 24, 2023, in Aalborg, The Department of Materials and Production at Aalborg University, Fibigerstræde 16, 9220 Aalborg, Room 1.208

Looking forward to seeing you in Aalborg

On behalf of the organizers

Morten Bilde Simonsen
Aalborg University

Gold sponsor

AnyBody Technology is a pioneer and leading provider of mechanical modeling of the living body, in particular musculoskeletal modeling. The all-dominating area of application is of course the human body, but our technology applies to analysis of any creature – currently living, pre-historic, or imaginary. Our base technology is the AnyBody Modeling System™ – the simulation engine – and the AnyBody Managed Model Repositories for instance containing the world's most comprehensive human full-body musculoskeletal model.

Silver sponsor

Velamed GmbH, based in Cologne, Germany, is a leading medical distribution company specializing in biomechanical measuring systems. We excel in equipping laboratories with tailored solutions through close collaboration with technology leaders, ensuring customer-oriented innovation

Program overview

09:00 – 09:30	Poster Mounting, Registration, Coffee
09:30 – 09:45	Welcome by the organizers and sponsors
09:45 – 10:25	Podium Presentations
10:25 – 11:10	Keynote by Enrico de Pieri
11:10 – 11:25	Break
11:25 – 12:55	Student competition sponsored by AnyBody Technology
12:55 – 14:00	Lunch
13:05 – 14:00	General assembly
14:00 - 15:10	Podium presentations
15:10 – 15:20	Student award ceremony
15:20 – 16:20	Posters and coffee
16:20 – 17:00	Beer, soda, snacks and networking

Keynote lecture

Enrico de Pieri

Enrico De Pieri is a senior research engineer at Zimmer Biomet, Winterthur, Switzerland, where he's developing and validating novel musculoskeletal modelling approaches to gain deeper insights into the biomechanics of healthy, pathological, and surgically reconstructed joints. His primary objective is to improve the lives of patients affected by musculoskeletal conditions and restore their mobility.

He earned his PhD in 2019 from the Institute for Biomechanics at ETH Zurich, where he investigated the variability in implant loading experienced by patients with total hip replacements during various activities of daily living. Throughout his tenure as a postdoctoral researcher at ETH Zurich and as a research associate at the University of Basel Children's Hospital, Enrico investigated the role of limb (mal-)alignment on the onset and progression of various musculoskeletal disorders. His research spanned a spectrum of conditions including increased femoral anteversion, miserable malalignment syndrome, overuse injuries, hip impingement, and joint osteoarthritis. Additionally, he developed musculoskeletal modelling tools that supported surgeons in interpreting clinical gait data of orthopaedic and neuro-orthopaedic patients, particularly those affected by conditions such as cerebral palsy. Concurrently, he held the role of lecturer in clinical biomechanics at the University of Basel.

Organizing Committee

Morten Bilde Simonsen. Aalborg University

John Rasmussen, Aalborg University

DBS Board

Scientific Committee

Fatih Alibeyoglu, Samsun University, Türkiye

Moustafa Mesbah, University of Mostaganem, Algeria

Ryuji Shigemitsu, Tohoku University Graduate School of Dentistry, Japan

Ilias Theodorakos, Aalborg University, Denmark

Diego Martinez Echevarria, Aalborg University, Denmark

Matin Afshar, Aalborg University, Denmark

Morten Bilde Simonsen, Aalborg University, Denmark

Detailed program

09:00 – 09:30	Poster Mounting, Registration, Coffee
09:30 – 09:45	Welcome by the organizers and sponsors. By John Rasmussen, AnyBody Technology and Velamed
09:45 – 10:25	**Podium Presentations 1**
09:45 – 09:55 Page: 12	What are we talking about? a pilot review of injury risk inferences in biomechanical experiments of running Sebastian Deisting Skejø
09:55 – 10:05 Page: 13	Predicting drag in a racing kayak using a forward dynamics model Jonas Østergaard Juhl, Mark de Zee and Kent Klitgaard
10:05 – 10:15 Page: 14	Persons with parkinson's disease show repeated bout rate enhancement during cycling Ernst A. Hansen, Mathilde J. C. Berner, Nikoline H. Gade, Maja H. Bjørnkjær, Anders F. Brekke, Vibeke Grønlund
10:15 – 10:25 Page: 15	The effect of power clean or loaded hex bar jump on physical performance in soccer Sebastian Svane, Mathias Kristensen Chair: Mark de Zee
10:25 – 11:10	**Keynote by Enrico de Pieri** Increased femoral anteversion in children – can musculoskeletal modeling better inform clinical decision-making? Chair: John Rasmussen
11:10 – 11:25	Break

11:25 – 12:55	**Student competition sponsored by AnyBody Technology**
11:25 – 11:35 Page: 16	Investigating the validity and reliability of the repone velocity sensor on average concentric velocity in squat and bench press Marcus Thrane Leth, Tue Skallgaard and Louise Fleng Sandal
11:35 – 11:45 Page: 17	Analyzing one-repetition-maximum predictions: load-velocity relationship vs. repetition to failure equation in ten lower extremity exercises Mikkel Faarup, Jonas Green Jensen, Sissel Rosenkrans Pedersen, Rasmus Toftholm Jakobsen, Elisa Jolas, Michael Skipper Andersen, Mathias Kristiansen, Morten Bilde Simonsen
11:45 – 11:55 Page: 18	Biomechanical gait analysis of overground walking in healthy individuals using robot-assisted dynamic body weight unloading Jon Skovgaard Jensen, Anders Holsgaard-Larsen, Anders Stengaard Sørensen, Per Aagaard, Jens Bojsen-Møller
11:55 – 12:05 Page: 19	Impact of an upper limb exoskeleton on muscle activity during three task Musso Matteo, A. S. Oliveira and S. bai
12:05 – 12:15 Page: 20	Effects of in field use and familiarization of a passive back exoskeleton on the lower back muscles during logistics work Lasse Schrøder Jakobsen, Mark de Zee Afshin Samani, Kévin Desbrosses, and Pascal Madeleine
12:15 – 12:25 Page: 21	Bones segmentation from lower extremity mri for patient-specific modeling Yunsub Jung, Morten Blide Simonsen and Michael Skipper Andersen
12:25 – 12:35 Page: 22	Effects of transcranial direct current stimulation combined with arm swing on the walking performance of people with parkinson's disease Vinicius Cavassano Zampier, P.I. Bichara, P.P. Gutierres, F.A. Barbieri, A. S. Oliveira

12:35 – 12:45 Page: 23	Gait kinematics during body weight support in young adults with neurological disorders Morten B. Pedersen, Per Aagaard, Anders Stengaard Sørensen, Gitte Rasmussen and Anders Holsgaard-Larsen
12:45 – 12:55 Page: 24	Towards a laxity protocol for in vivo applications: Preliminary results parameters Brett Michael Musolf, Ilias Theodorakos, Michael Skipper Andersen Chair: Peter Christian Raffalt
12:55 – 14:00	Lunch
13:05 – 14:00	General assembly
14:00 - 15:10	**Podium presentations 3**
14:00 – 14:10 Page: 25	Advancing orthopaedic postoperative evaluation through time-series 3d computed tomography: focusing on femoral torsion Ahmed Haloum, Ole Rahbek, Søren Kold, Jan Rölfing, Shima Gholinezhad, John Rasmussen, Ahmed Abood
14:10 – 14:20 Page: 26	The determination of the optimal material combination for total hip prosthesis components using parametric finite element analysis I. Ağıl, Fatih Alibeyoglu and A.T. Şensoy
14:20 – 14:30 Page: 27	Lean mass and isometric upper body strength are associated with sprint kayak performance Mathias Kristiansen, Matthew Flood and Kent Klitgaard
14:30 – 14:40 Page: 28	Patient-specific spinal bone screw fixation: homogenized versus voxel-based finite element analysis Mohammadjavad Einafshar, Alireza Rouyin, Mohadese Rajairad, Mohammadjavad Salmani, Farzam Farahmand, Navid, Arjmand

14:40 – 14:50 Page: 29	A preliminary analysis on the feasibility of detecting gait events using machine learning and motion sensors embedded in smartphones Larsen, Aske G., Sadolin, Line Ø., Thomsen, Trine R., Oliveira, Anderson S.
14:50 – 15:00 Page: 30	Children diagnosed with idiopathic toe walking – altered treatment strategy when 3d-gait analysis is added to the decision-making Anders Holsgaard-Larsen, Tina Udemark Pasgaard, Sidsel Hald Rahlf, Julie Ladeby Erichsen, Bjarke Viberg, Christian Færgemann
15:00 – 15:10 Page: 31	Biomechanical efficacies of stabilization of lumbar degenerative diseases using hybrid instrumenations: a finite element study Moustafa Mesbah, Mohamed Bendoukha, Abdelwahed Berkaoui, Hakim Chiali
	Chair: Michael Skipper Andersen
15:10 – 15:20	**Student award ceremony**
15:20 – 16:20	**Posters and coffee**
#1 Page: 32	Prediction of discrete football actions using semi-supervised machine learning Larsen, Aske Gye, Papi, Giovanni & Oliveira, Anderson Souza
#2 Page: 33	Kinematic analysis of the two phases, jump on trampette and trampette support phase, with focus on angles and angular velocity in the lower body. Østerballe, Nielsen, W. Nielsen & K. Nielsen,
#3 Page: 34	Evaluation of trip-reducing elements using a mechanical free body shoe collision test Mathias Munk-Hansen, Anders Holsgaard-Larsen, Mark de Zee, Thor Grønlykke, Pascal Madeleine

#4 Page: 35	AnyBody modeling driven by multi-modal data from wearable sensors Mingyuan He, Shaoping Bai
#5 Page: 36	Biomechanical Evaluation of Lumbar Interbody Fixation Techniques: A Comparative Study of Standalone Cages vs. 360-Fixation Constructs Ali Kiapour, Mohammadjavad Einafshar, Elie Massaad, John Shin
#6 Page: 37	Modulating femoral torsion: evaluating the impact of a novel plate design in a growing porcine model Ahmed Haloum, Ole Rahbek, Søren Kold, Jan Rölfing, Shima Gholinezhad, John Rasmussen, Ahmed Abood
#7 Page: 38	Quest for Accuracy: Progressing Towards Optimal Ultrasound Settings for Bone-Soft Tissue Interface Identification Martin Vorup Lindvand, Nico Verdonschot, Ilias Theodorakos, and Michael S. Andersen
#8 Page: 39	Sensitivity analysis of cartilage creep material properties prediction in unconfined compression: impact of data quantity Bo E. Seiferheld and Michael S. Andersen
#9 Page: 40	Robot-assisted weight relief for prevention of musculoskeletal pain among bronchoscopists Knudsen PK, Jepsen RB, Sørensen AS, Juul AD, Andersen JF, Deleuran MK, Dalager T, Søgaard K
#10 Page: 41	Classification of jaw movements from tmd patients based on pca Ryuji Shigemitsu, Takehiko Mito, Emika Sato, Hiroshi Egusa, Keiichi Sasaki and John Rasmussen
16:20 – 17:00	Beer, soda, snacks and networking

Abstracts

WHAT ARE WE TALKING ABOUT? A PILOT REVIEW OF INJURY RISK INFERENCES IN BIOMECHANICAL EXPERIMENTS OF RUNNING

Sebastian Deisting Skejø[1,2]
[1]Department of Public Health, Aarhus University, Denmark; sdsk@ph.au.dk
[2]Research Unit for General Practice, Aarhus, Denmark

INTRODUCTION

Running-related injuries are a biomechanical phenomenon: no injuries can occur without biomechanical tissue load causing tissue damage [1]. The imposed biomechanical load is determined by a multitude of factors, such as running technique, speed and equipment, that can be accurately measured and characterised in biomechanical experiments. However, the degree to which such experiments explains the risk of actually sustaining a running-related injury is debatable. Is it, for instance, reasonable to conclude that a change in running technique that leads to increased peak ankle net joint moments also leads to increased ankle injury risk, if the same technical change, in practice, also causes runners to run shorter distances? In this pilot study, I review, I investigate whether and how biomechanists infer effects on running-related injury risk from biomechanical findings in experiments.

METHODS

On October 11th, 2023, I searched PubMed for `running AND (biomech* OR kinematic* OR kinetic*)`. The search was limited to articles published after January 1st, 2022 to narrow the scope of this pilot study. Subsequently, I scanned the titles and abstracts of all search results and excluded articles outside the scope of this review. My inclusion and exclusion criterias were intended to provide a representative overview of the recent biomechanical literature related to running, yet still limit the scope to a feasible pilot study. Thus, I elected to only include peer-reviewed original articles studying biomechanics of steady state running written in English. Further limiting the scope, I only included articles that reported spatiotemporal parameters (e.g. step length or frequency), segment or joint kinematics, ground reaction forces, joint kinetics or kinetics of individual anatomical structures. Articles were excluded if they concerned sprinting, acceleration, non-linear running or other test modalities (e.g. jumping). I also excluded studies that included physiological testing (e.g. VO_2 measurements) and injury studies in an attempt to ensure that my findings were representative of the biomechanical community and not of those whose expertise is within physiology or epidemiology.

Once articles were included, I read the methods, results, discussion and, where applicable, conclusion and implications sections of each article. In some cases, this reading led to the exclusion of further articles. For the remaining included articles, I extracted the reported biomechanical outcomes and any inference to injury risk in the discussion, conclusion or implications. Depending on the wording used, I classified these inferences as "none" if injury risk wasn't mentioned at all, "non-association" if authors directly warned against inferring injury risk from their results, "potential association" if authors suggested that their results may inform injury risk or "strong association" if authors directly encouraged runners/clinicians to alter running based on their findings. I continued reading articles until I had included a total of 20 articles.

RESULTS AND DISCUSSION

The initial search returned 1,077 articles of which 222 articles were included after scanning titles and abstracts. Subsequently, I excluded 11 articles after reading them. The findings of the 20 included articles are summarized in Table 1.

Although, my review of the literature is limited by its small sample size and the risk of bias stemming from a single reviewer, it is appears that injuries are an important part of biomechanical running research, as most of the reviewed studies suggest potential or strong associations between their biomechanical findings and injury risk. In the studies, such inferences are typically based on mechanistic logic ("all else being equal" a higher biomechanical load leads to higher injury risk) or by referring to previous epidemiological studies. However, both approaches have limitations and judging whether or not these injury risk inferences are approriate is likely a somewhat subjective.

Two approaches that I may help approriately infer injury risk from biomechanical experiments in the future are using frameworks that incorporate both training habits, biopsychosocial factors and biomechanics [2] and working cross-disciplinary with e.g. epidemiologists [3].

REFERENCES

[1] Edwards, WB. *Exerc Sport Sci Rev* **46**:224-231, 2018
[2] Nielsen RO et al. *Br J Sport Med* **54**:941, 2020
[3] Bahr R, Krosshaug T. *Br J Sport Med* **39**:324-329, 2005

Table 1 Summary of findings from the 20 included articles. Note that the number of articles reporting biomechanical outcomes is higher than the total for each level of injury risk inference, as a single article may report outcomes in multiple categories.

Inferred association to injury risk	Number of articles reporting biomechanical outcome					Total
	Spatiotemporal parameters	Ground reaction force	Segment or joint kinematics	Joint kinetics	Structure kinetics	
None	3	1	2	2	-	5
Non-association	1	1	1	1	1	2
Potential	5	4	9	4	3	11
Strong	-	1	1	1	1	2

PREDICTING DRAG IN A RACING KAYAK USING A FORWARD DYNAMICS MODEL

Jonas Østergaard Juhl[1], Mark de Zee[1] and Kent Klitgaard[1]

[1] ExerciseTech, Department of Health Science and Technology, Aalborg University, Aalborg, Denmark;

INTRODUCTION

A numerical model is presented with the goal to analyze surge kinematics exhibited by racing kayaks. The model implements the most relevant physics, and is therefore very general. It serves as a foundational framework for forthcoming investigations into parameter studies.

METHODS

Let x denote traveled distance. By Newton's 2nd law of motion, the acceleration is given by the second order differential equation:

$$x'' = \mathrm{Acc}(t, x') = \frac{F_{Net}(t,x')}{(m+m_{Add})} \quad (1)$$

where F_{Net} is the net force acting on the kayak, t is elapsed time, m is the total mass of the paddler and kayak and m_{Add} is the added mass, consisting of deflected water by the hull. The total drag force is calculated as

$$R = R_F + R_P + R_W + R_A \quad (2)$$

where R_F is the skin friction drag component, R_P is the form drag component, R_W is the wave making drag component and R_A is the air drag component.

The skin friction drag coefficient is calculated with the ITTC-1957 friction line CF = 0.075/(Log(Re)-2)² and with the wetted surface area estimated by a hull constructed in a Cartesian coordinate system. The starboard/port water-lines and the bottom longitudinal centerline are described by quadratic polynomials and the hull is a quadratic polynomial in any transversal cross section (see Figure 1).

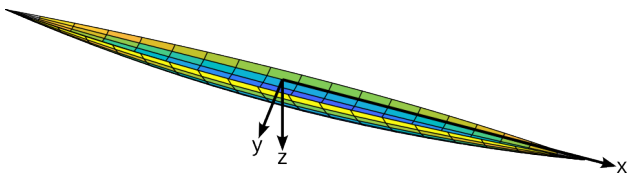

Fig. 1 *The hull, used to estimate the wetted surface area.*

The wetted surface area is then calculated based on the immersed volume. The form drag coefficient is estimated with the Prohaska method on a CFD model. The wave making drag is estimated by the Michell's integral [3] on a Wigley hull and the air drag is estimated with a log wind profile. An overview of the different types of drag contributions is presented in Figure 2.

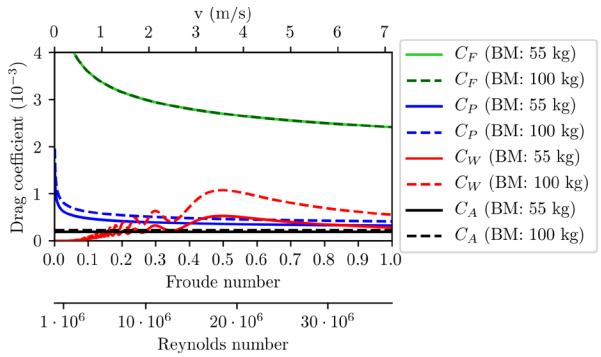

Fig. 2 *The drag coefficients in the present study with respect to the wetted surface area, for two different body masses.*

Propulsion force is modeled with piecewise power functions as seen on Figure 3. To solve (1) the 4th order Runge-Kutta method is applied.

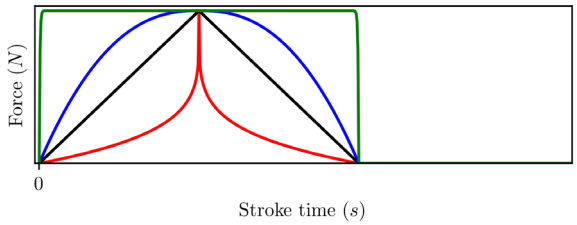

Fig. 3 *Four different stroke profiles shown, with different average stroke forces.*

RESULTS AND DISCUSSION

For validation, the model is compared to experimental results in Figure 4.

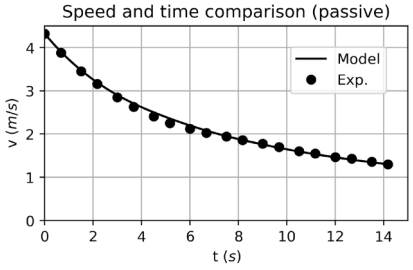

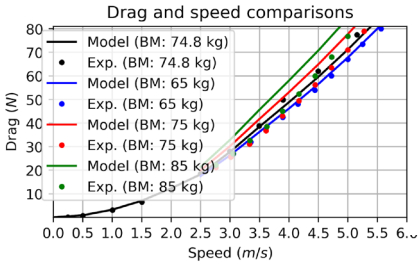

Fig. 4
a) *The drag force of the model compared to experimental towing data [3,4].*

b) Comparison of the model to experimental data of passive speed relative to time.

Overall, the model predicted drag is on par with experimentally measured drag. The model predicts higher drag, than experimental measured by Gomes et al. [3] (BM: 65 kg, BM: 75 kg and BM: 85 kg). Contrary, the model prediction for BM: 74.8 kg was lower than the experimentally measured by Tzabiras et al, whereby the model predictions lie in between the findings of the different authors.

CONCLUSIONS

A forward dynamic driven model of racing kayak surge kinematics was successfully established, which shows good agreement with experimental data. Nevertheless, it is suggested that further validation, with particular emphasis on the active speed scenario, should be undertaken.

REFERENCES

1. J. H. Michell. *Philosophical Mag.* **45**: 106–123, 1898.
2. Georgios D. Tzabiras et al., *The Sport J.* **13**: 4, 2010.
3. Beatriz Gomes et al., *Sports Biom.* **14**: 394-403, 2014.
4. Charlie Prétot et al., *Applied Sciences* **12**: 8925, 2022.

PERSONS WITH PARKINSON'S DISEASE SHOW REPEATED BOUT RATE ENHANCEMENT DURING CYCLING

Ernst A. Hansen[1], Mathilde J. C. Berner[1], Nikoline H. Gade[1], Maja H. Bjørnkjær[1], Anders F. Brekke[1], Vibeke Grønlund[2]

[1]Centre for Health and Rehabilitation, University College Absalon, Slagelse, Denmark. [2]Knowledge and competency center for rehabilitation for persons with Parkinson's, Sano Skælskør and The Danish Parkinson Association, Denmark

INTRODUCTION

The main purpose of the present study was to test whether the motor behavioural phenomenon of repeated bout rate enhancement (as previously reported for index finger tapping [1, 2] and cycling [3] in healthy recreationally active individuals) also occurs in persons with Parkinson's disease during submaximal ergometer cycling. In the present context, repeated bout rate enhancement is defined as an increase of the freely, or spontaneously, chosen cadence applied during repeated bouts of cycling. This is for example relevant to study since the phenomenon is suggested to reflect an exercise-triggered net excitation of the part of the nervous system that controls rhythmic movement [3], and Parkinson's disease is a central nervous system disorder that affects the neuromotor control [4].

METHODS

Persons (n=8, 6 men, 2 women, 1.75±0.07 m, 77.4±12.9 kg, 69.6±12.4 years) with idiopathic Parkinson's disease (Hoehn & Yahr stage 2-3 [5]) first performed an incremental test to find the submaximal power output, which resulted in a Borg scale [6] value of 10 or above. This test resulted in power output of 60±14 W and a Borg scale value of 11±1. On a later day, the participant performed five consecutive 5-min bouts of submaximal ergometer cycling at the individual predetermined power output. The bouts were separated by 10-min rest periods. All cycling was performed on a Monark 928 G3 cycle ergometer (Monark Exercise AB, Vansbro, Sweden) and cadence was freely chosen. Participants were blinded to cadence. Cadence was noted every 30 s. Subsequently, a single value of the freely chosen cadence was calculated, as a mean across the noted values during the last 3 min, and used for further analysis. Heart rate was monitored with a Polar H9 chest strap and the Polar Team app (Polar Electro Oy, Kempele, Finland) and noted every 30 s. Subsequently, a single value of the heart rate was calculated as a mean across the noted values during the last 3 min, for further analysis. Borg scale value was noted after each bout. Participants were all on medication for Parkinson's disease and in the clinical state "ON" during all testing. Data are reported as average±standard deviation. $p \leq .050$ was considered statistically significant.

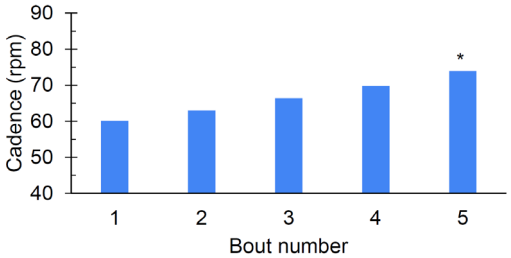

*Freely chosen cadence as a function of bout number. n=8. Cycling bouts lasted 5 min each, and were separated by 10-min rest periods. *Different from the value during 1. bout (p=.019).*

RESULTS

The main result was that cadence at the end of the 5. bout (74±21 rpm) was statistically significantly (p=.019) higher (26%±29%) than at the end of the 1. bout (60±18 rpm). The gradual increase across the five bouts is illustrated in the figure. The heart rate amounted to 107±16 and 113±21 beats per min at the end of the 1. and 5. bout, respectively (p=.182). The Borg scale value was 10±1 and 12±3 at the end of the 1. and 5. bout, respectively (p=.037).

DISCUSSION AND CONCLUSION

Parkinson's disease is a degenerative condition of the brain that affects the affected person's neuromotor control. For example, it is generally considered that the disease results in slow movements.

Indeed, the cadence at the end of the 1. bout was on average about 8 rpm lower for the participants in the present study as compared to healthy recreationally active participants in a previous study (68±18 rpm) [3].

However, for a direct comparison of the present main finding, we have previously reported an average of 15% of repeated bout rate enhancement in recreationally active individuals during submaximal cycling at an intensity resulting in about 10 on the Borg scale [3]. In the present study it amounted to an average of 26% - a considerable larger value. Thus, if any difference from recreationally active individuals, it might look like persons with Parkinson's disease show a more - rather than less - pronounced degree of the repeated bout rate enhancement phenomenon.

It has been suggested that the repeated bout rate enhancement phenomenon occurs because of a nonconscious rhythmogenesis process. A neuromodulation in form of a net excitation of relevant parts of the nervous system might explain the increased cadence [3].

The present findings might have relevance for the understanding of the neuromotor control of automated rhythmic movement in persons with Parkinson's disease as well as for development of effective and enjoyable cadence-focused cycling training for these persons.

In conclusion, the motor behavioural phenomenon of repeated bout rate enhancement during submaximal ergometer cycling was observed in the present study. Thus, the freely chosen cadence was increased by on average 26%, corresponding to 14 rpm, as accumulated values across five consecutive 5-min bouts of ergometer cycling.

REFERENCES

1. Hansen EA *et al.* (2015) J Mot Behav **47**:490-96
2. Mora-Jensen M *et al.* (2017) Motor Control **21**:457-67
3. Smith A *et al.* (2022) Int J Exerc Sci **15**:1142-55
4. Alberts JL & Rosenfeldt AB (2020) J Parkinsons Dis **10**(s1):S21-S27
5. Hoehn MM & Yahr MD (1967) Neurology **17**:427-42
6. Borg G (1970) Scand J Rehab Med **2**:92-98

THE EFFECT OF POWER CLEAN OR LOADED HEX BAR JUMP ON PHYSICAL PERFORMANCE IN SOCCER

Sebastian Svane[1] and Mathias Kristiansen[1]

[1]ExerciseTech, Department of Health Science and Technology, Aalborg University, Aalborg, Denmark

INTRODUCTION

Olympic lifts, such as the power clean, are a vital part of soccer strength training programs to enhance power output of the lower extremities and are frequently used as physical performance tests (1). However, the power clean is a very complex and technically demanding exercise as the high velocity of the barbell makes the coordination of the lift and catch phase very difficult. The athlete will also need to possess high degrees of flexibility in the wrists, knees, ankles and hips to perform the power clean correctly. Consequently, it can take many years for soccer athletes to master the exercise and reap the associated performance enhancing benefits. Contrary, the loaded hex bar jump imitates the exact same movement pattern of the power clean without the high complexity and technical demands (1,2). The aim of the present study was therefore to investigate the effect of a seven-week strength training intervention in soccer players using either the power clean exercise or loaded hex bar jump in enhancing physical performance.

METHODS

Twenty-two U17 elite soccer players (height = 182.5±5.1 cm, body mass = 70.0±5.2 kg) underwent a seven-week strength training intervention with performance tests before and after. The athletes were stratified into a hex bar training group (HX) or a power clean group training (PC) based on their pretest results. Testing on day one day consisted of measuring maximal power output in the 61 kg and 81 kg loaded hex bar jump test, power clean one repetition maximum and countermovement jump. Day two consisted of a 10- and 25-meter sprint test and a 505 change of direction test. All tests were carried out before and after the training intervention.

The training intervention consisted of seven weeks of supervised training in power clean or loaded hex bar jump. The training was performed twice a week with at least 48 hours between sessions. The PC group performed power clean while the HX group performed loaded hex bar jumps followed by their normal training routine. The volume performed in power clean and loaded hex bar jumps was equated between groups.

RESULTS AND DISCUSSION

A paired t-test showed a significantly higher CMJ ($p<0.001$), power clean 1RM ($p<0.001$), higher power output for loaded 81 kg hex bar for both the HX and PC group ($p<0.001$) and a slower 10-meter sprint speed ($p=0.02$) for PC group. An unpaired t-test revealed no significant differences in any of the physical performance tests between groups at either pre or posttest. It appears that both exercises target the lower body triple extension of the ankle, knee and hip in a similar fashion and therefore lead to a similar degree of transferability to the performance tests (3). The decrease in 10-meter sprint time for PC group and lack of increase in change of direction speed could be explained by an increase in accumulated fatigue over the season, as the pretest was performed shortly after a recovery winter break, while the post test was performed mid-season between one or twice weekly soccer matches (3). This could indicate that the loaded hex bar jump training intervention may have countered the negative effect off in season fatigue as no change in sprint time were found from pre to post-test (3).

CONCLUSIONS

In conclusion, both power clean and loaded hex bar jump training were effective in enhancing physical performance in the performance tests. No significant differences in performance were found between HX and PC groups in any of the tests.

REFERENCES

1. Oranchuk, DJ, et al., *The Journal of Strength & Conditioning Research,* **33.1:** 17-24, 2019.
2. Teo, SY, et al., *journal of strength and conditioning research*, **30**.10:2741-2748, 2016.
3. Ne´de´lec, M, et al., *sports medicine*, **42**: 997-1015,2016

Table 1 *An overview of physical performance measures pre- and post-test results including the p-value between tests in the following exercises. The loaded hex bar jump 61- and 81kg, power clean one repetition maximum, counter movement jump height, 505 change of direction test and 10- and 25 meter sprint time. * Indicates a significant difference between pre and posttest.*

	Hexbar jump group			Power clean group		
	Pre-test	**Post-test**	**P-value**	**Pre-test**	**Post-test**	**P-value**
Loaded hex bar jump 41 kg.	574.6±91.01W	586.3±95.7W	0.58	527.3±58.6W	559.9±32.8W	0.16
Loaded hex bar jump 81 kg.	576.4±100.1W	751.1±65.4W	<0.001*	564.9±62.8W	701.8±84.3W	<0.001*
Power clean	53.9±8.6kg	58.9±8.9kg	<0.001*	51.9±6.5kg	60.6±7.3kg	0.006
Counter movement jump	34.3±3.5cm	41.4±4.8cm	<0.001*	33.9±3.7cm	38.4±3.9cm	<0.001*
Change of direction	2.38±0.04s	2.34±0.11s	0.34	2.43±0.12s	2.37±0.12s	0.14
10-meter sprint	1.84±0.07s	1.87±0.07s	0.28	1.82±0.07s	1.88±0.05s	0.02
25-meter sprint	3.70±0.09s	3.73±0.12s	0.08	3.71±0.08s	3.77±0.12s	0.13

INVESTIGATING THE VALIDITY AND RELIABILITY OF THE REPONE VELOCITY SENSOR ON AVERAGE CONCENTRIC VELOCITY IN SQUAT AND BENCH PRESS

Marcus Thrane Leth*[1], Tue Skallgaard[1] and Louise Fleng Sandal[1]

[1] University of Southern Denmark, Department of Sports Science and Clinical Biomechanics.
*Student, Marcus email: Malet19@student.sdu.dk

INTRODUCTION

Implementing velocity-based measures in resistance training offers several benefits [1]. However, the reliability and validity of technologies for measuring barbell velocity require further clarification, particularly in specific exercises.

This study aimed to investigate the criterion validity and test-retest reliability of the linear position transducer, RepOne, during submaximal squat and bench press.

METHODS

Eleven well-trained participants (10 males and 1 female) performed submaximal muscle strength repetitions of squat and bench press while using the RepOne transducer to estimate barbell velocity.

To assess criterion validity, RepOne was compared to a gold standard for position, Vicon, using a correlation analysis and paired t-test. Participants performed 2 sets of 1 repetition of 70% 1RM in the squat.

Test-retest reliability was assessed by examining biases in Bland-Altman plots and calculating the coefficient of variation (CV). Participants performed 2 sets of 2 repetitions of 70% of 1RM in bench press and squat.

RESULTS AND DISCUSSION

The results showed a very strong correlation (r=0.997) between average concentric velocity (ACV) as measured by Vicon and RepOne (Figure 1). The correlation between Vicon and RepOne closely aligns with the equivalence line, indicating no systematic bias. Validity was further supported by a paired t-test, which found no statistically significant difference between RepOne ACV and Vicon ACV ($p = 0.151$). The average difference between the measurement devices was 0.004 m/s (±0.006 m/s), which is considered negligible in a physical training context.

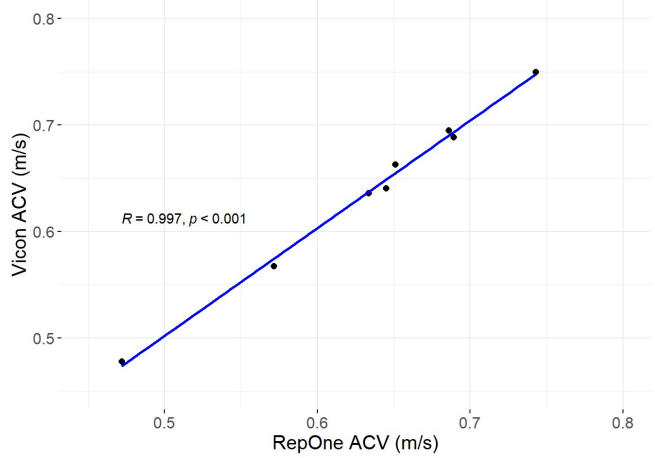

Fig. 1 Correlation analysis of Vicon and RepOne ACV with associated Pearsons r.

Test-retest reliability was high, as indicated by negligible biases in squat and bench press ACV, with values of +0.012 m/s and -0.001 m/s, respectively (Figure 2 and 3). These differences are considered negligible and attributed to human variance. The CV, which represents relative variation, for squat ACV was 2.8%, and for bench press ACV, it was 4.3%. The low CV values indicate a low relative variation in ACV.

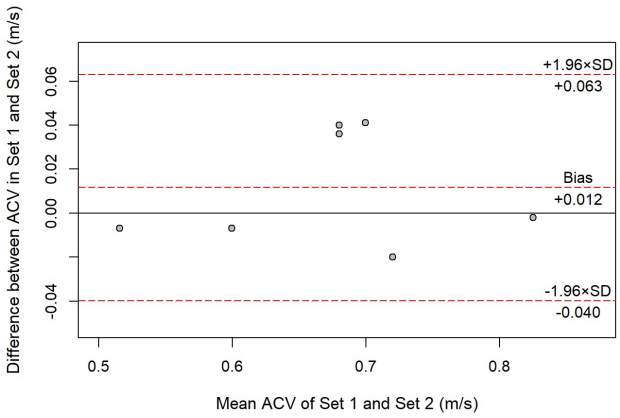

Fig. 2 Bland-Altman plot for Squat ACV

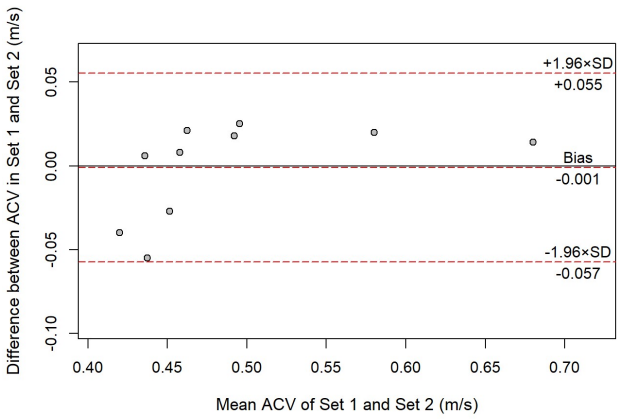

Fig. 3 Bland-Altman plot for Bench Press ACV

CONCLUSIONS

Overall, RepOne exhibited strong validity and test-retest reliability for measuring ACV in squat and bench press in well-trained participants.

REFERENCES

1. Thompson SW, et al. *Sports* **8**, 94, 2020

Analyzing One-Repetition-Maximum Predictions: Load-Velocity Relationship vs. Repetition to Failure Equation in Ten Lower Extremity Exercises

Mikkel Faarup*[1], Jonas Green Jensen*[1], Sissel Rosenkrans Pedersen*[1], Rasmus Toftholm Jakobsen*[1], Elisa Jolas*[,2,3,4], Michael Skipper Andersen[3,4], Mathias Kristiansen[1], Morten Bilde Simonsen[3,4]

[1]Department of Health Science and Technology, Aalborg University, [2]Ecole Normale Supérieure de Rennes, [3]Center for Mathematical Modeling of Knee Osteoarthritis, [4]Department of Materials and Production, Aalborg University.
*Student

INTRODUCTION

Assessment of maximal strength is commonly used to profile an individual's physical capacities, and the one-repetition maximum (1RM) test is among some considered the gold standard for dynamic muscle strength [1]. 1RM is the maximum external load an individual can lift for a single repetition in an exercise [2]. 1RM testing is a valuable tool with wide-ranging practical applications in the training and rehabilitation of athletes, clients, and patients. However, frequent 1RM testing is time-consuming, physically and psychologically taxing, difficult to get reliable results in untrained, and problematic to perform in a rehabilitation setting, limiting its practicality in some cases [3,4]. Therefore, different sub-maximal tests have emerged, like the repetitions until-failure test, where submaximal loads (e.g., 85% of 1RM) are lifted until fatigue, and regression formulas are used to estimate a 1RM load [3]. However, a relatively recent approach is emerging, which allows prediction of 1RM based on only a few repetitions at relatively low loads [5]. The technique relies on the observed inverse linear association between the lifted load and the concentric velocity of a repetition, known as the load-velocity relationship. The aim of the present study was to investigate the concurrent validity of a measured 1RM compared to the 1RM estimated from either the load-velocity relationship or the repetitions until-failure test in ten lower extremity exercises.

METHODS

A total of 22 healthy participants were recruited. The tested exercises included ankle, knee, and hip joint flexion and extension, as well as hip abduction, hip adduction, and leg press. Velocity during the concentric phase was measured using a linear transducer, and individual linear regression models were established using approx. 5 submaximal loads (40-80% 1RM) and velocity to estimate the 1RM. Furthermore, multiple equations presented by McNair et al. 2011 were used to estimate the 1RM based upon the repetition to failure test. Intraclass correlation coefficient (ICC) and normalized mean absolute error (NMAE) was used to compare the measured 1RM, with the estimated 1RM from both the load-velocity and the repetition to failure test.

RESULTS AND DISCUSSION

Predictions based on the load-velocity relationship exhibited NMAE values ranging from 8.1% to 33.7%, and ICC values from 0.30 to 0.9 (Table 1). Among the fatigue estimation equations, the Lombardi equation demonstrated the lowest NMAE across all exercises (5.8%), with an excellent ICC of 0.99 and narrow limits of agreement. The present study showed that the NMAE between the measured and predicted 1RM from the load-velocity relationship was high, and the limits of agreement were very wide. As such, predicting the 1RM in lower extremity resistance exercises from the load-velocity relationship is not considered to exhibit high concurrent validity. On the other hand, the Lombardi equation showed low NMAE, narrow limits of agreement, and high ICCs values. However, this was not the case for all equations.

Table 1: Evaluation of 1RM prediction based on the load-velocity relationship.

Exercise	NMAE (%)	ICC	1RM load [kg]
Ankle dorsiflexion	28.8±6.3	0.31±0.24	18.1 ± 4.1
Seated plantarflexion	15.6±1.5	0.70±0.09	110.0 ± 23.6
Plantarflexion	33.7±8.2	0.30±0.27	65.2 ± 17.7
Hip abduction	16.4±2.8	0.73±0.10	15.0 ± 4.4
Hip adduction	16.0±1.2	0.78±0.04	14.4 ± 3.4
Hip extension	22.6±2.2	0.56±0.09	21.1 ± 6.4
Hip flexion	17.5±2.3	0.51±0.11	16.1 ± 3.9
Knee extension	12.7±1.7	0.87±0.04	27.1 ± 9.7
Knee flexion	23.5±4.4	0.57±0.12	15.5 ± 4.7
Leg press	8.1±1.5	0.90±0.05	103.2 ± 31.1

1RM = 1 Repetition Maximum; NMAE = Normalized Mean Absolute Error; ICC = Intra-class Correlation Coefficient.

CONCLUSIONS

The load-velocity relationship proved inadequate for predicting 1RM in lower-extremity single-joint exercises. However, the Lombardi estimation equations showcased favorable predictive performance with a consistently low average NMAE across all exercises studied.

REFERENCES

1. Grgic J, Lazinica B, Schoenfeld BJ, Pedisic Z. Sports Med Open 2020;6:
2. Verdijk LB, Van Loon L, Meijer K, Savelberg HHCM. J Sports Sci 2009;27:59–68.
3. McNair PJ, Colvin M, Reid D. Arthritis Care Res (Hoboken) 2011;63:216–222.
4. Hughes LJ, Banyard HG, Dempsey AR, Scott BR. J Strength Cond Res 2019;33:2409–2419.
5. Jidovtseff B, Harris NK, Crielaard JM, Cronin JB. The Journal of Strength & Conditioning Research 2011;25:267–270.

Biomechanical Gait Analysis of Overground Walking in healthy individuals using Robot-assisted Dynamic Body Weight Unloading

Jon Skovgaard Jensen[1] (jskovgaard@health.sdu.dk), Anders Holsgaard-Larsen[1], Anders Stengaard Sørensen[2], Per Aagaard[3], Jens Bojsen-Møller[3]

[1]Orthopaedic Research Unit, Department of Clinical Research, University of Southern Denmark.
[2]Health Informatics and Technology, The Maersk Mc-Kinney Moller Institute, University of Southern Denmark.
[3]Muscle Physiology and Biomechanics Research Unit, Department of Sport Science and Clinical Biomechanics, University of Southern Denmark.

Ph.D.-Student

INTRODUCTION

Body weight unloading (BWU) involves vertical upwards force application to the body centre of mass, which reduces kinetic requirements of lower limb joints during walking [1]. In order to ensure task-specificity during neurorehabilitation, BWU systems should provide an appropriately modulated force that allows biomechanically undistorted gait patterns. No studies were found investigating to which extent a BWU system applying an instantly modulated force, supports 'normal' kinematic and kinetic gait patterns using time-continuous analysis. Unlike statistical analysis of discrete variables, statistical parametric mapping of the entire signal-trajectories allows statistical inference regarding changes in movement patterns across different levels of unloading [2,3]. In the present study, a novel robot-assisted BWU technology, designed to continuously modulate the unloading force was employed to achieve undistorted gait patterns of the individual.

The aim of the present study was to evaluate the extent to which kinematic, kinetic and spatiotemporal parameters are affected by robot-assisted modulated BWU in young healthy adults during overground walking at a self-selected speed.

METHODS

Twenty participants walked barefoot at self-selected speed in a 3-D motion-capture lab (VICON Inc., Oxford, UK, 8*T40 and 8*T20 cameras, 200 Hz sample rate) at 0, 10, 20, 30, 40, and 50% BWU. Vertical and horizontal ground reaction forces (GRFs) (AMTI, Watertown, MA, USA, 1000 Hz sample rate) and lower limb internal joint moments were obtained, by means of standard Plug-in-gait methodology, from the stance phase, while joint angles were obtained from entire strides (gait cycles). Kinematic and kinetic trajectories were time-normalised using linear interpolation. Spatiotemporal parameters were extracted as discrete variables. Time-continuous data were analysed using Statistical Parametric Mapping (SPM) [2] to compare different BWU conditions by means of One-Way Repeated Measures Anova univariate analyses.

RESULTS AND DISCUSSION

With increasing BWU, progressive reductions were observed for GRFs (e.g., Vertical GRF Figure 1), internal joint moments, joint angles, walking speed, stride/step length and cadence.

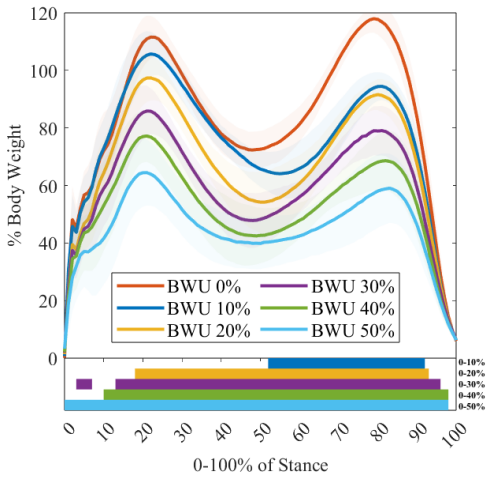

Fig. 1 Vertical Ground Reaction Force obtained during stance at 0, 10, 20, 30, 40, and 50% BWU (group mean). Bottom panel: Bars represent phases of statistically significant signal differences relative to 0% BWU.

With increasing BWU levels, participants walked at slower self-selected speed, with shorter and wider steps, lower cadence, reduced joint range of motion and reduced kinetic requirements of lower limb joints. While amplitude reductions were observed for kinetic and kinematic variables across the time-domain, the relative trajectory shapes remained largely preserved (cf. Figure 1).

CONCLUSIONS

In conclusion, instantly and continuously modulated robot-assisted BWU yields reduced kinetic requirements without distorting the basic shape of biomechanical gait patterns during overground walking in young healthy adults. Robot-assisted BWU may be of relevance in rehabilitation of patients with gait impairments, and BWU systems yielding an instantly modulated force may be superior to BWU systems with less dynamic/rapid force-feedback mechanisms.

REFERENCES

1. MacLean, M.K., Ferris, D.P., 2021. Human muscle activity and lower limb biomechanics of overground walking at varying levels of simulated reduced gravity and gait speeds. PLOS ONE 16, e0253467. https://doi.org/10.1371/journal.pone.0253467
2. Pataky, T.C., 2010. Generalized n-dimensional biomechanical field analysis using statistical parametric mapping. J. Biomech. 43, 1976–1982. https://doi.org/10.1016/j.jbiomech.2010.03.008
3. Pataky, T.C., 2016. rft1d: Smooth One-Dimensional Random Field Upcrossing Probabilities in Python. J. Stat. Softw. 71, 1–22. https://doi.org/10.18637/jss.v071.i07

IMPACT OF AN UPPER LIMB EXOSKELETON ON MUSCLE ACTIVITY DURING THREE TASK

Musso Matteo[1,*], A. S. Oliveira[1] and S. bai[1]

[1] Department of Material and Production, Aalborg University, Aalborg, 9220, Denmark

* Ph.D. student, mmus@mp.aau.dk

INTRODUCTION

Exoskeletons for upper limb support have gained increasing attention as a potential solution for addressing shoulder musculoskeletal disorders (MSDs). These devices can reduce muscle activity, joint perceived discomfort, and effort around the shoulder region [1]. Previous studies primarily focus on tasks performed with a shoulder flexion angle of around 90°. Shoulder MSDs may already occur during extended or repetitive activities involving shoulder flexion angles below 60° but above 20° [2]. In this study, we aim to assess the impact of an upper limb exoskeleton on muscle activity during common tasks of the construction and manufacturing sectors performed not only at shoulder level: overhead assembly, bricklaying, and box-moving tasks.

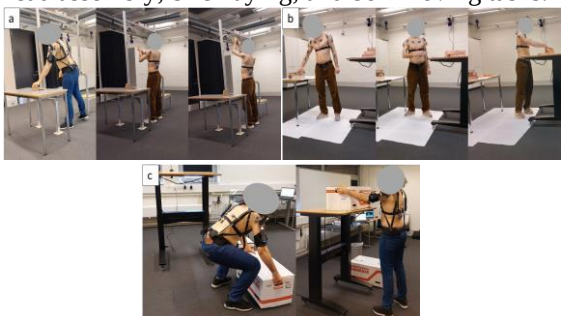

Fig. 1 The three tasks tested in the study. (a) Overhead assembly, (b) bricklaying, and (c) box moving.

METHODS

The exoskeleton used in the study was the Skelex 360 (Skelex, Rotterdam, The Netherlands). It is a passive device with an adjustable support level ranging from 0.5 to 3.5 kg and 2.7 kg weight. During the study, the support force of the device was adjusted for every subject to compensate for their arm weight. Eighteen healthy males participated in the study and performed three tasks: overhead assembly (T1), bricklaying (T2), and box-moving (T3). All the tasks were repeated three times in two conditions, with and without the exoskeleton. During overhead assembly, Fig 1.a, participants placed ten screws into an aluminum profile whose height was set to ensure that participants started screwing with their dominant shoulder and elbow flexed at 90°. For the bricklaying, Fig 1.b, participants transferred ten 2 kg bricks from a table to a second whose height was adjusted to the participants' navel height. A pace of 15 rpm was. During the box-moving, Fig 1.c, participants moved a 10 kg box from the floor to the top of a table at a pace of 15 rpm. Eight muscles were targeted during the experiment on both sides for EMG assessment: anterior (AD), middle (MD), and posterior (PD) deltoids, biceps brachii (BB), brachioradialis (BRA), pectoralis major (PM), latissimus dorsi (LD), and erector spinae longissimus (ERL). After the acquisition, the EMG data of target muscles were segmented to highlight the activation bursts using the method proposed by [3]. The AD segments were used on the same side muscles of the overhead assembly. For the bricklaying and box moving, the AD was used for ì the shoulder muscles, the BRA for itself, and the BB, the ERL for itself. Following segmentation, the RMS of the activation burst was calculated and normalized by the MVC. Finally, the average activation level across participants was computed for each muscle and condition. The difference in muscle activation between conditions was computed and expressed as a percentage of the mean MVC.

RESULTS AND DISCUSSION

The results of our analysis are summarized in Table 1. The results obtained during the overhead assembly show the effectiveness of this exoskeleton in supporting repetitive quasi-statistic tasks performed overhead. All recorded shoulder flexor muscles presented a significant decrease in activity, with a maximum of -6.69% on the non-dominant side AD. Using the exoskeleton also decreased the activity of the investigated shoulder extensor muscles (i.e., PD and LD). During the bricklaying activity, the exoskeleton reduced the activity of the AD and MD. The increased activity found for the PD might be attributed to the participants having to stop the exoskeleton in the phase of increasing support. The AD and MD activity was significantly reduced on both sides when the exoskeleton was used during the box moving task. Increased activity was found for the PD and LD.

Table 1 Differences in muscle activation with and without exoskeletons (expressed as MVC percentage) for the work tasks. Notes: Highlighted statistical significance and decreases (green) or increases (red). D: dominant side, ND: non dominat side. BRA data was not reported; no significant difference was found in any task.

		Muscles						
		AD	MD	PD	BB	PM	LD	ERL
T1	D	-3.41	-2.11	-0.49	-0.65	-2.7	-0.33	-0.79
	ND	-6.69	-1.78	-0.63	-1.54	-3.21	-0.21	-0.62
T2	D	-1.64	-0.82	0.47	0.45	-0.83	0.06	0.48
T3	D	-7.65	-1.73	2.02	1.6	0.005	1.43	1.68
	ND	-4.37	-2.91	0.81	-0.42	0.38	1.42	-.002

CONCLUSIONS

These findings suggest that applying an exoskeleton for performing these tasks might be beneficial to support the shoulder, as the overall muscular activation around that joint was reduced.

REFERENCES

1. de Vries A, et al., The effect of arm support exoskeletons in realistic work activities: A review study, *J Ergonomics* **9:255**, 2019
2. McAtamney L, et al., RULA: a survey method for the investigation of work-related upper limb disorders, *Applied Ergonomics* **24**: 91-99, 1993
3. Yang D, et al., Accurate EMG onset detection in pathological, weak and noisy myoelectric signals, *Biomedical Signal Processing and Control* **33**: 306–315 2017

Effects of in field use and familiarization of a passive back exoskeleton on the lower back muscles during logistics work

Lasse Schrøder Jakobsen[1*], Mark de Zee[1] Afshin Samani[1], Kévin Desbrosses[2], and Pascal Madeleine[1]

[1]Exercise Tech, Department of Health Science and Technology, Aalborg University, Denmark

[2]The French National Research and Safety Institute for the Prevention of Occupational accidents and Diseases, Nancy, France

*PhD student

INTRODUCTION

Occupational exoskeletons are an attractive solution to lower the physical load of logistic workers since reduced muscle activity has been reported as an effect of exoskeleton assistance [1]. Especially back-supporting exoskeletons are of interest, as back pain represents the largest contributor to attrition and sick leave among manual workers [2]. Yet, field studies investigating the effects of familiarization are very rare despite the development of unobstructive sensors [3]. The aim of this field study was to investigate the changes in muscle activity when using a passive back exoskeleton and how these changes were affected by familiarization.

METHODS

Twenty workers from a Danish logistics company (30.3 ± 8.2 years, 177.9 ± 12.1 cm, 81.1 ± 15.6 kg) were randomly assigned to a control (CON) and an intervention (INT) group. The workers underwent a pre- and post-test separated by an intervention period of five weeks. During the intervention period the INT group were included in a familiarization protocol comprising introduction and training using the passive back exoskeleton (V3 BackX-S, SuitX by Ottobock, PBE), and five weeks of progressive in field PBE use (7.5h/week → 37h/week). The test sessions included lifting boxes (4.6 kg, 10.0 kg, and 17.6 kg) from a 15 cm shelf to a 100 cm truck in a movement inducing trunk flexion and rotation. All lifting tasks were conducted four times with and without PBE assistance in a randomized order. Full-body 3D kinematics were recorded using IMU-based motion capture (Xsens Awinda, Fs: 60 Hz) and muscle activation of erector spinae were estimated using surface electromyography (SEMG) recordings (Noraxon, Fs: 1500 Hz). A maximum voluntary isometric contraction (MVC) procedure was performed by all workers [4]. All tasks were rated by the workers using a Borg CR10 scale to estimate the rate of perceived exertion (RPE). The full wave SEMG signals were segmented to the movement using the kinematics, before being filtered and normalized to MVC. The 90th percentiles of the rectified SEMG amplitude were calculated. A two-way RM-ANOVA was conducted to assess the effects of use and familiarization of the PBE.

RESULTS

Using the PBE significantly reduced the level of muscle activity of erector spinae (left and right) during the lifting tasks among the workers ($p < .002$) (Fig. 1). Furthermore, the RPE also decreased with PBE assistance ($p < .05$). Interactional effects of familiarization and PBE use were found during the 4.6 kg ($p = .023$) and 17.6 kg lift ($p = .020$), pointing at decreased muscle activity of right erector spinae from pretest to posttest among INT (Fig. 2).

DISCUSSION AND CONCLUSIONS

The SEMG results underline the capability of the PBE towards lowering the muscle activity of the lower back, supported by the decreases in RPE. Furthermore, the results indicate that the exoskeleton becomes more effective when getting familiarized to the device, which is an effect suggested in other areas of research as well [5]. These findings underline the potential benefits of exoskeleton use in the logistics sector and the importance of familiarization as a part of implementation of exoskeleton.

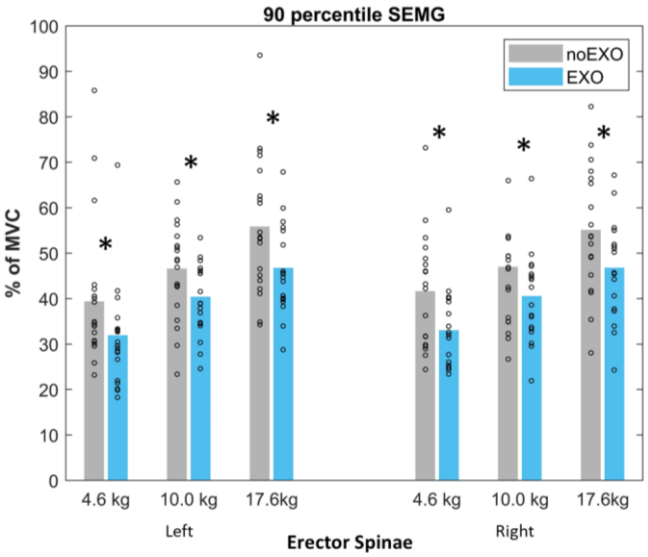

Fig 1. Mean and individual values of the 90th percentile SEMG amplitude of left and right erector spinae during noEXO/EXO conditions. *Indicates significant differences ($\alpha < .05$).

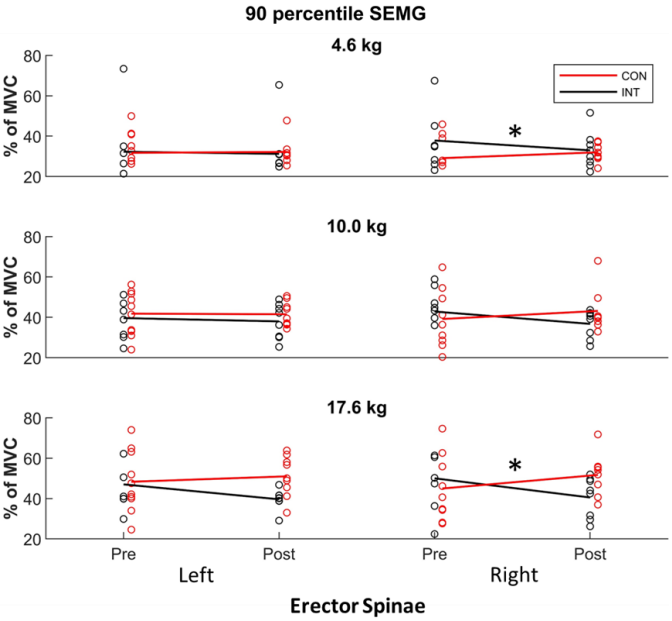

Fig. 2. Mean and individual values of the 90th percentile SEMG amplitude of left and right erector spinae of CON and INT group during EXO condition from the pre/posttests. *Indicates significant differences ($\alpha < .05$).

ACKNOWLEDGEMENTS

The project was funded by Dagrofa Logistics A/S, who also provided facilities, personnel, equipment, and general organizational support.

REFERENCES

1. Theurel J & Desbrosses K., IISE TOEHF, 2019.
2. Govaerts R, et al., BMC Musculoskelet. Disord., 2021.
3. Nussbaum MA, et al., IISE TOEHF, 2019.
4. Vera-Garcia FJ, et al., J Electromyogr. Kinesiol., 2010.
5. Diamond-Ouellette G, el al., IISE TOEHF, 2022.

BONES SEGMENTATION FROM LOWER EXTREMITY MRI FOR PATIENT-SPECIFIC MODELING

Yunsub Jung[1,2*], Morten Blide Simonsen[1,2] and Michael Skipper Andersen[1,2]
[1]Department of Materials and Production, Aalborg University, Denmark
[2]Center for Mathematical Modeling of Knee Osteoarthritis, Aalborg University, Denmark
*Ph.D.student, yunsubj@mp.aau.dk

INTRODUCTION

Medical imaging is widely used in the field of biomechanics to construct patient-specific musculoskeletal models [1]. In particular, magnetic resonance imaging (MRI) provides the most comprehensive evaluation of geometries, joint damage, and osteoarthritis and is a good multi-plane image for soft tissue contrast [2]. However, manual segmentation of human structures is a time-consuming and labor-intensive task and a bottleneck for future advancements in the field. This study presents a method to extract bones from lower extremity MRI images automatically.

METHODS

The total number of segmentation target bones is 10 (pelvis, femur, tibia, patella, and tarsal). Lower extremity MRI images (field strength 1.5T, sequence: T1-fl2d) stitched into three or four scans were used. A multi-atlas-based method was used to segment bones, and a total of 27 atlas data sets were created through manual segmentation. Among these, 9 atlas data were finally selected considering image quality and registration performance. All atlas data include information on manually marked bone regions and the original MRI images.

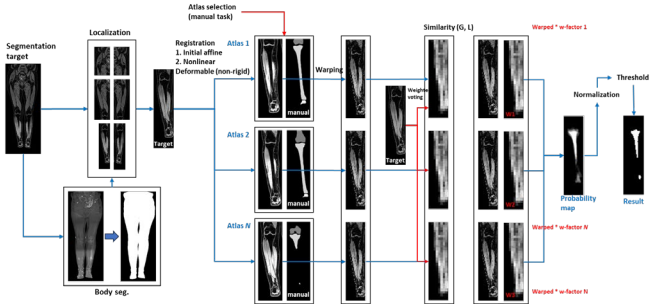

Fig. 1 Schematic diagram of the segmentation algorithm

Segmentation proceeded in the following steps: atlas selection, segmentation of body surface, localization, image registration using a pyramid model, similarity computation between target and atlas image, and weighted voting (Fig. 1). Body surface information was used to reduce the amount of computation when computing the registration and similarity. In addition, the number of iterations of the pyramid model was determined by considering the segmentation results and computation time. The 10 bones finally segmented have different label values in the image, and the segmentation results for each bone were quantitatively compared with manual segmentations. Four metrics (sensitivity, specificity, accuracy, and precision) were used for quantitative comparison.

RESULTS AND DISCUSSION

Table 1 shows the segmentation results according to the similarity criterion. The two similarity criterion methods showed similar results but different performances depending on the bone segmented. It is known that the pelvis shapes in males and females are different. Atlas-based segmentation is based on the morphological information of the target object. However, our atlas data did not distinguish between male and female pelvis. In the future, we plan to improve this through additional research.

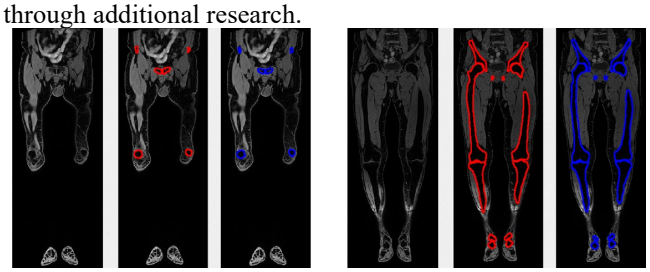

Fig. 1 Segmentation results: original image (left), manual marking (middle), segmented result (right)

CONCLUSIONS

Atlas-based methods have shown good overall performance for bone segmentation, but expansion of the atlas set is required for the pelvis.

REFERENCES

1. Satanik M., et al. *Front in Bioe Biot* **8**: 1-20, 2020
2. Qi L., et al. *Imaging* **8**: 418-28, 201

Table 1 Experimental results

SC*	Metric	Left					Right				
		Tibia	Femur	Pelvis	Patella	Tarsal	Tibia	Femur	Pelvis	Patella	Tarsal
NMI	Sensitivity	0.771	0.526	0.279	0.696	0.360	0.714	0.631	0.258	0.715	0.564
	Specificity	0.997	0.988	0.999	0.999	0.994	0.997	0.994	0.999	0.998	0.994
	Accuracy	0.991	0.966	0.986	0.991	0.964	0.990	0.977	0.985	0.991	0.974
	Precision	0.866	0.703	0.771	0.925	0.757	0.849	0.853	0.782	0.896	0.837
NCC	Sensitivity	0.772	0.526	0.281	0.692	0.351	0.714	0.631	0.262	0.717	0.561
	Specificity	0.997	0.988	0.999	0.999	0.994	0.997	0.994	0.999	0.998	0.994
	Accuracy	0.991	0.966	0.986	0.991	0.964	0.990	0.977	0.985	0.991	0.973
	Precision	0.867	0.703	0.771	0.925	0.756	0.851	0.852	0.784	0.899	0.835

Note.-NMI = normalized mutual information, NCC = normalized cross correlation
*Similarity criterion

EFFECTS OF TRANSCRANIAL DIRECT CURRENT STIMULATION COMBINED WITH ARM SWING ON THE WALKING PERFORMANCE OF PEOPLE WITH PARKINSON'S DISEASE

Vinicius Cavassano Zampier[1,2,*], P.I. Bichara[1], P.P. Gutierres[1], F.A. Barbieri[2], A. S. Oliveira[3]

[1] São Paulo State University (UNESP), Posture and Gait Studies Laboratory (LEPLO); [2]São Paulo State University (UNESP), Human Movement Research Laboratory (MOVI-LAB); [3]Department of Materials and Production, Aalborg University
*Ph.D. Student

INTRODUCTION

Transcranial direct current stimulation (tDCS) and physical exercise are relevant methods to reduce gait deficits in people with Parkinson's disease (PwPD), as increase stride length and stride velocity [1]. Another method to improve gait performance in PwPD is to increase arm swing amplitude and frequency during walking [2]. However, it is unknown whether combining tDCS and arm swing during walking would generate greater adaptations when compared to performing only arm swing. Therefore, the aim of the present study was to determine whether a combined tDCS and physical exercise (e.g., arm swing) intervention improves walking performance of PwPD.

METHODS

Fifteen PwPD (age: 70,87±6.4 years) were recruited to participate in this randomized, double blind, sham controlled, cross over clinical trial. Participants were tested in two days. In day one, participants received a 20-minute tDCS stimulation with a current intensity at 2mA (Active), whereas in the second day participants received a Sham 10-second stimulation throughout a 10-minute interval. Stimulations were elicited by placing the anode electrode over the participant's motor cortex contralateral to the most affected side and the cathode electrode the over supra orbital area contralateral to the anode. The two test days (active or sham) were randomized for each participant. On both days and concomitantly to the stimulation protocol, participants performed a 20-minute walking protocol. Participants were instructed to walk over an 8-m walkway while increasing their arm swing range of motion (10 minutes) and while increasing their arm swing speed (10 minutes).

Before and after the 20-minute intervention on the Active and Sham days, walking performance was assessed by instructing participants to walk through an 8-m walkway where a carpet with pressure sensors (GaitRite) was located. Participants were instructed to walk over the walkway five times, and walking performance was estimated using averaged walking stride length and stride velocity. The effects of group (Active *vs* Sham) and time (pre *vs* post intervention) were assessed using a two-way ANOVA with repeated measures. The statistical level was set at $p<0.05$.

RESULTS AND DISCUSSION

There was a main effect of time for stride length ($F_{1,28}$= 62,089; p<0,001; η_p^2= 0,689) and stride velocity ($F_{1,28}$= 59,831; p<0,001; η_p^2= 0,681). Participants increased their stride length (Figure 1) and stride velocity (Figure 2) following both the Active and Sham interventions, with no difference between groups for stride length and stride velocity (p>0.05). These results corroborate previous studies demonstrating improvements in the walking performance of PwPD following gait training [3]. Such type of intervention increases sensory stimulus, improve spatial perception and motor response [3]. However, we found no differences between Active and Sham interventions, conversely to previous literature that demonstrated superior effects of tDCS combined with gait training in walking performance [4]. It is likely that a single session of stimulation is not enough to elicit relevant effects on walking performance.

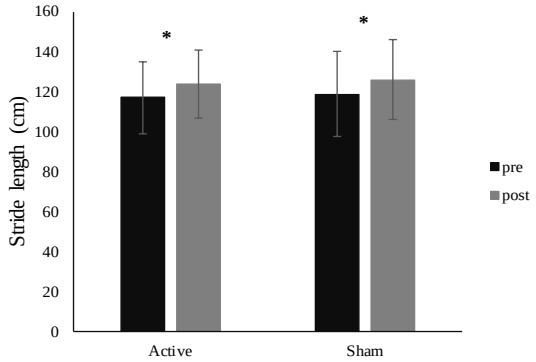

Fig. 1 Mean±SD stride length for the Active and Sham groups pre (*black bars*) and post intervention (*gray bars*). *significant difference between pre and post (p<0,001).

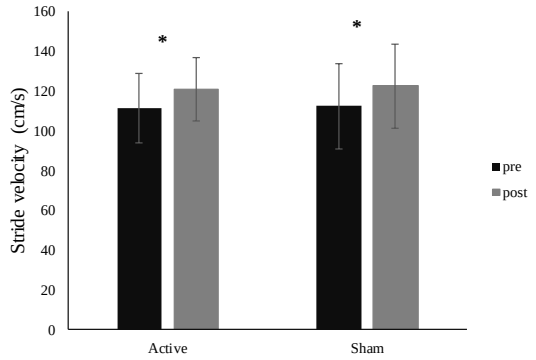

Fig. 2 Mean±SD stride velocity for the Active and Sham groups pre (*black bars*) and after intervention (*gray bars*). * significant difference between pre and post (p<0,001).

CONCLUSIONS

Our results suggest that both combined tDCS/arm swing intervention and a simple arm swing intervention led to improvements in walking performance. However, the lack of differences between the two interventions suggests that a greater number of tDCS sessions are needed to elicit improvements in walking performance.

REFERENCES

1. Fatame P, et al. The effects of tDCS on gait in patients with PD: a systematic review, Translational neurodegeneration 10.1 (2021): 1-19.

2. Zampier VC, et al Gait bradykinesia and hypometria decrease as arm swing frequency and amplitude increase. Neuroscience Letters 687 (2018): 248-252.

3. Shulman LM., et al. "Randomized clinical trial of 3 types of physical exercise for patients with Parkinson disease." JAMA neurology 70.2 (2013): 183-190.

4. Costa-Ribeiro A, et al. "Transcranial direct current stimulation associated with gait training in Parkinson's disease, Developmental neurorehabilitation 20.3 (2017): 121-128

Gait kinematics during body weight support in young adults with neurological disorders

Morten B. Pedersen[1,2,*], Per Aagaard[3], Anders Stengaard Sørensen[4], Gitte Rasmussen[5] and Anders Holsgaard-Larsen[1,2]

[1]Department of Orthopaedics and Traumatology, Odense University Hospital, [2]Department of Clinical Research, University of Southern Denmark, [3]Department of Sports Science and Clinical Biomechanics, University of Southern Denmark, [4]The technical faculty, University of Southern Denmark [5]Department of Culture and Language, University of Southern Denmark
*Ph.D. student, mlyngpedersen@health.sdu.dk

INTRODUCTION

Body weight supported (BWS) gait training has frequently been used in the functional rehabilitation of adults with neurological disorders. Ideally, BWS reduces the user's apparent body weight while supporting vertical alignment and lateral stability in given ambulation tasks, hence allowing gait training of higher quality and safety [1]. To ensure task-specificity during neurorehabilitation, BWS systems should provide an appropriately modulated force that support biomechanically normal movement patterns. However, no knowledge exists concerning the impact of robot assisted BWS during different levels of modulated force on gait kinematics in this population.

Hence, the objective was to investigate the impact of robot assisted BWS on kinematic gait parameters, by employing different levels of modulated force during overground walking in young adults with neurological disorders.

METHODS

Kinematic data were obtained in 18 young adults with neurological disorders during overground gait at a self-selected pace at six different levels of modulated BWS. Changes in sagittal hip, knee, and ankle angle trajectories were analysed as time-series data using Statistical non-Parametric Mapping (SnPM) to compare different levels of BWS in one-way ANOVA analyses. To further explore these findings, post-hoc SnPM t-tests were performed, comparing 0% BWS to 10-50% BWS.

RESULTS AND DISCUSSION

Statistical non-Parametric Mapping (SnPM) repeated measures ANOVA analyses of sagittal hip, knee, and ankle angle trajectories indicated changes between the six body weight support levels (0%, 10%, … , 50% unloading). These differences were mainly located in the initial loading phase, pre swing, mid-swing, and terminal swing phases of the gait. Post-hoc SnPM t-tests indicated an increased impact on angle trajectories with increasing support levels. Post-hoc multivariate analysis of amplitude and temporal effects indicated that gait kinematics were impacted in terms of both amplitude and timing.

CONCLUSIONS

Applying adaptive (modulated) body weight support during overground gait impacted sagittal gait kinematics by inducing: *(i)* Changes in hip, knee and ankle angles during initial loading, pre swing, mid-swing and terminal swing phases, (*ii*) higher levels of body weight support had larger impact on gait kinematics, *(iii)* both amplitude and timing of gait kinematics were affected.

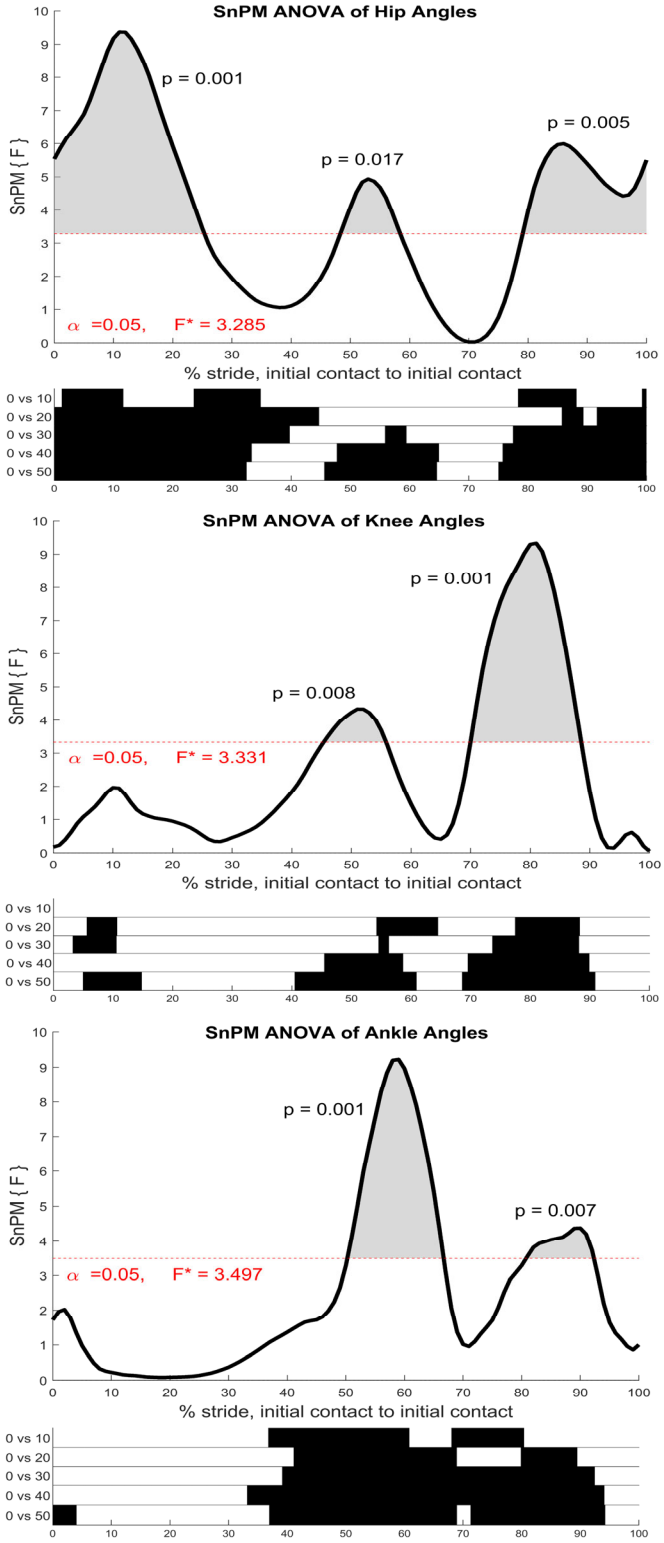

Fig. 1: Statistical non-Parametric Mapping (SnPM) repeated measures ANOVA of sagittal hip, knee, and ankle angle trajectories. Black bars indicate differences ($p<0.05$) in the gait cycle based on post-hoc SnPM t-testing comparing 0% unloading with 10-50% BWS levels.

REFERENCES

1. Apte S, et al. Influence of body weight unloading on human gait characteristics: a systematic review. *Journal of NeuroEngineering and Rehabilitation*. **15**(1): 53, 2018

Towards a laxity protocol for in vivo applications: Preliminary results parameters

Brett Michael Musolf[1,*], Ilias Theodorakos[1], Michael Skipper Andersen[1]
[1]Center for Mathematical Modeling of Knee Osteoarthritis, Department of Materials and Production, Aalborg University
* Ph.D. student

INTRODUCTION

The state-of-the-art in knee laxity testing is mechanized load application devices paired with X-rays measuring bone translations and rotations [1]. These devices have a capacity for gauging laxity in single directions, however, they give limited information for determining the properties of individual ligaments. While it has been shown to be possible to determine these properties through laxity tests, the number of load combinations and the resulting X-ray exposure make this infeasible *in vivo* [2]. In this study, we, therefore, propose and evaluate a selection protocol that requires a few laxity tests to determine ligament properties.

METHODS

A subject-specific tibiofemoral model was developed in the AnyBody Modeling System (AMS v 7.5.0, Aalborg Denmark) using magnetic resonance imaging (MRI) scans of a healthy participant. The model was comprised of the femur and tibia bones, their articular surfaces, and the ligaments. Only the cruciate and collateral ligaments of the knee were modeled from these scans. These ligaments were modeled as single-dimensional, non-wrapping elements following a non-linear force-strain behavior. [2]. The properties of the ligaments–stiffness (k) and reference strain (ε_r)–were initially set according to existing literature values [2]. The femur was fixed in space, while the tibia was connected to the femur in a predefined knee flexion angle. The remaining five degrees of freedom (DOF) were modelled as force-dependent kinematics (FDK) DOFs [3].

A synthetic laxity profile was generated using this model by applying the following forces and moments on the tibia segment: anterior forces were applied on the tibial tuberosity with magnitudes varying from -150 to 150 [N] in steps of 15 [N], and varus and internal rotation moments were applied on the tibia with magnitudes varying from -10 to 10 [Nm] in steps of 2 [Nm]. These ranges were repeated at 0°, 30° and 60° of knee flexion. The resulting knee kinematics were computed by allowing the joint to balance under the influence of the external loads and the internal loads (ligaments forces and articular surfaces contact forces) using the FDK solver [3]. The resulting displacements and rotations of the knee, as well as the resulting force and strain uniquely experienced by each ligament were computed for each scenario.

We defined a protocol by choosing three laxity trials per ligament: the trial that resulted the highest, the second highest and half the highest ligament force. Following that procedure, we obtained a protocol with twelve laxity trials defined by knee flexion, applied load, and resulting joint kinematics.

We then evaluated this protocol by using it to determine the ligament properties of two different participants using their respective subject-specific knee models and synthetic laxity profiles. An optimization routine was employed to match the knee kinematics of the synthetic laxity profiles by altering the ligament parameters. The Complex optimization algorithm was employed to solve the problem. It used a population of twenty candidate solutions randomly generated around the ground truth ligament values within a box of [-500, 500] [N] and [-0.02, 0.02] [] for stiffness and reference strain, respectively. The optimized ligament parameters were compared against the respective ground truth values to evaluate the performance of the protocol.

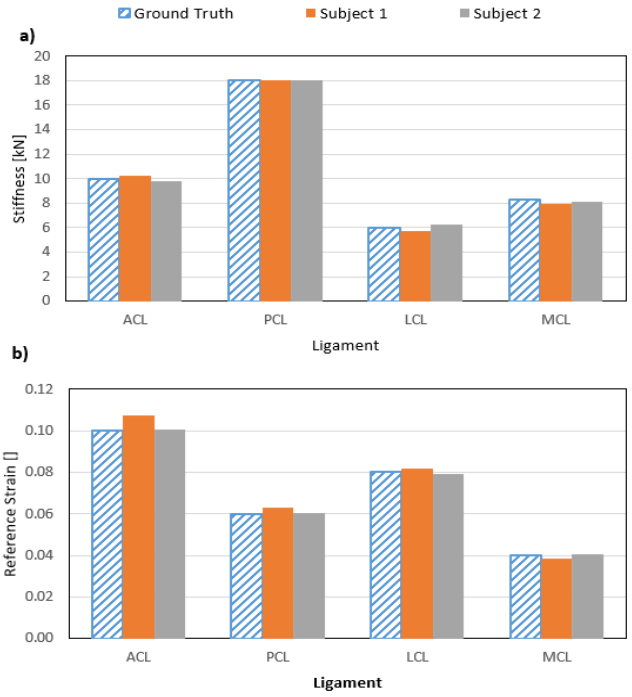

Fig. 1 The final values of the a) stiffness and b) strain of the anterior cruciate ligament (ACL), posterior cruciate ligament (PCL), lateral collateral ligament (LCL), medial collateral ligament (MCL) after the optimization procedure

RESULTS AND DISCUSSION

A root mean square error of 0.03 [N] and 0.02 [N] for stiffness and 0.05 [] and 0.01 [] for the reference strain were observed for participants 1 and 2, respectively. The results, as shown in Figure 1, show that the employed methodological procedures allowed us to predict the ligament parameters accurately.

CONCLUSIONS

Despite the small sample size, this study demonstrates promising results towards the development of a laxity protocol for *in vivo* applications. Future studies should evaluate its robustness to experimental inaccuracies and optimization choices such as the initial guess.

REFERENCES

1. J. Kümmerlin et al. *J. Biomech. Eng* **144**(8): 1-7, 2022
2. M. S. Andersen et al. *J. Biomech. Eng* **143**(6), 2021
3. M. S. Andersen et al. *J. Biomech. Eng* **139**(9), 2017

Advancing Orthopaedic Postoperative Evaluation through Time-series 3D Computed Tomography: Focusing on Femoral Torsion

Ahmed Haloum[1], Ole Rahbek[1], Søren Kold[1], Jan Rölfing[2], , Ahmed Abood[2], Shima Gholinezhad[1,3], John Rasmussen[3]

[1]Department of Orthopaedic Surgery, Aalborg University Hospital, Denmark
[2]Department of Clinical Medicine - Orthopaedic surgery, Aarhus University, Denmark
[3]Department of Materials and Production, Aalborg University, Denmark

INTRODUCTION

In the realm of orthopedics, there is an essential need for image-based evaluation of rotational growth (1). Traditionally, Orthopedic surgical assessments predominantly rely on 2D/2D registration of time-series Computed Tomography (CT) images, whether single or superimposed, but they inherently have limitations in accurately assessing complex rotational deformities in long bones. These limitations arise from variations in defining the reference line on axial images through manual landmark selection, resulting in inconsistent torsion angle measurements, reducing reliability and inter-rater agreement in 2D-CT methods (2). Additionally, these methods primarily focus on a single imaging plane, potentially overlooking rotational changes in other planes, inevitably caused by orthopedic interventions.

In tackling these challenges, 3D/3D surface registration emerges as a potential solution by facilitating comprehensive three-dimensional bone assessments without the necessity of landmark selection, as it considers the integration of all surface points (3). To explore this avenue, we have employed 3D modeling and specialized surface registration techniques and validated the efficency for the particular application of assessing the change of femoral torsion in a growing bone.

METHODS

Three-dimensional (3D) triangular surface models were generated from CT scans, each taken 12 weeks apart, of the right femurs in 11 pigs without any pathological conditions. For the quantification of femoral torsion, the registration-based approach commenced with initial superimposition of two images, allowing for the repositioning and rescaling of the 0 weeks bone to match the 12 weeks bone . In the next step, we performed sectioning of the modified 0 week bone, dividing it into two sections: one containing the femoral head and shaft (proximal), and the other encompassing the condyle (distal). Then, we implemented a surface registration algorithm to superimpose these sections onto their respective counterparts in the post-bone. Finally, we employed an affine decomposition technique, utilizing the derived transformation matrix from these registrations, to precisely determine the rate of rotation along distinct axes in various planes. To validate this method, we employed synthetic validation, carefully crafting controlled scenarios for assessing its performance and accuracy. This involved artificially introducing twists along three axes in the bones at specific angles and comparing the outcomes with known true values (twisting angles). Specifically, we applied the registration-based method to determine femoral torsion between twisted 12 weeks-bones from each pig and the 0 weeks bones of other pigs. This allowed us to assess the method's capability to accommodate the natural diversity among different bone structures.

RESULTS AND DISCUSSION

The validation outcomes demonstrated a close alignment between the detected angles and the true angles of 5, 10, 15, and 20 degrees, as evidenced by box plots illustrating detected angles for all 11 subjects across the three axes. Bland-Altman analysis further confirmed this alignment, showing minimal differences between the true angles and their corresponding detected angles across various true angles. The mean error was consistently near zero, with the limits of agreement defined by dashed grey lines indicating a narrow range. Despite the larger errors associated with larger true angles, the steady error percentage, suggests a relatively consistent relative accuracy across different true angles.

These results underscore the method's potential to enhance postoperative assessments, with significant implications for the evaluation of orthopaedic surgeries addressing corrective procedures like osteotomy and guided growth in the growing bone.

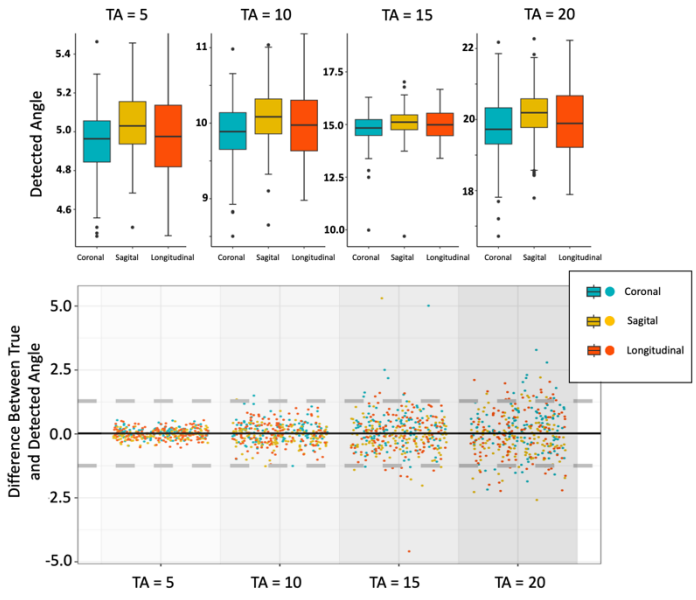

Fig. 1. An overview of validation results.

REFERENCES

1. P. B. Thippeswamy et al, “Updates in postoperative imaging modalities following musculoskeletal surgery,” J Clin Orthop Trauma,, Nov. 2021.
2. F. Schmaranzer et al,“The Effect of Modality and Landmark Selection on MRI and CT Femoral Torsion Angles,” Radiology, Aug. 2020.
3. Audette, Michel Aet al. "An algorithmic overview of surface registration techniques for medical imaging." Medical image analysis 4.3 (2000)

THE DETERMINATION OF THE OPTIMAL MATERIAL COMBINATION FOR TOTAL HIP PROSTHESIS COMPONENTS USING PARAMETRIC FINITE ELEMENT ANALYSIS

I. Ağıl[1*], F.Alibeyoglu[2*] and A.T. Şensoy[1]

[1]Samsun University, Faculty of Engineering, Department of Biomedical Engineering
[2]Aalborg University, The Faculty of Engineering and Science, Department of Materials and Production

INTRODUCTION

Accurate determination of the material properties of the components used in total hip prostheses (THP) is an important issue for the success of the prosthesis. Understanding the wear mechanisms that occur as a result of loads applied to the THP may help develop strategies that have the potential to reduce wear and extend the life of the implant. In this study, parametric finite element-based analysis (FEA) simulations were performed for THP components to determine the best combination among the material alternatives used in the literature. Thus, it is aimed to minimize the wear problem and implant loosening.

METHODS

In the first phase of the study, a solid femur model from the open-source design library GrabCAD [6] was imported into SolidWorks CAD software. The femoral head was osteotomized and implanted [7] using Virtual Surgery Planning (VSP).

Table 1: Mechanical Properties of Materials Used in Analysis Procedures

Material	Young Modulus (GPa)	Poisson Ratio
Ti30Nb5Sn5Zr [1]	48.3	0.36
Ti6Al4V [2]	110	0.342
CoCr [3]	250	0.3
CoCrMo [4]	230	0.3
Cortical Bone [5]	20.3	0.3
UHMWPE[2]	69	0.3
XLPE[3]	1	0.4

After defining the material properties obtained from the literature (Table 1), the assembly CAD model was transferred to ANSYS software, and a finite element model was established. The model, with its boundary conditions set, was then prepared for parametric analysis. The Taguchi experimental design, necessary for determining the parameter set, was conducted using Minitab statistical software. This process determined the number of analyses to be performed based on the number of factors and their levels. Within Minitab, considering the material selection for the hip implant, acetabular cup, and plastic liner, four different levels (candidate materials) were identified for these three factors, leading to a conclusion that 16 analyses would be conducted. The material properties of the components and the output parameters dependent on these properties (maximum equivalent von Mises stress of the implant and maximum total deformation of the implant) have been parametrically defined in ANSYS Workbench. The analysis was run and the result values for all design points were automatically obtained.

RESULTS AND DISCUSSION

In this study, FEA simulations were performed following the design combinations obtained by Taguchi experimental design depending on the different material combinations selected for THP components. According to these results, the lowest equivalent stress value for the hip implant-acetabular cup-plastic liner assembly was found in CoCr-Ti30Nb5Sn5Zr-Polyurethane components, respectively. In comparison, the lowest total deformation value was obtained for the material combination of CoCr-CoCr-UHMWPE. Table 2 shows the results of all design points suggested by the Taguchi approach.

Table 2: Results of the design points

Name	P1-Hip İmplant	P4-Acetabular Cup	P5-Plastic Liner	P2-Eq. Von Mises Stress- Hip Implant (MPa)	P6 Total Deformation Hip Implant (mm)
DP0	Ti30Nb5Sn5Zr	Ti30Nb5Sn5Zr	UHMWPE	745.53	11.52
DP1	Ti30Nb5Sn5Zr	Ti6Al4V	XLPE	729.17	11.6
DP2	Ti30Nb5Sn5Zr	CoCrMo	HDPE	745.34	11
DP3	Ti30Nb5Sn5Zr	COCr	Polyurethane	714.92	11.57
DP4	Ti6Al4V	Ti30Nb5Sn5Zr	XLPE	700.44	10.56
DP5	Ti6Al4V	Ti6Al4V	UHMWPE	723.12	10.49
DP6	Ti6Al4V	CoCrMo	Polyurethane	696.21	10.54
DP7	Ti6Al4V	COCr	HDPE	759.47	10.57
DP8	CoCrMo	Ti30Nb5Sn5Zr	HDPE	707.86	10.01
DP9	CoCrMo	Ti6Al4V	Polyurethane	681.55	9.99
DP10	CoCrMo	CoCrMo	UHMWPE	703.5	9.94
DP11	CoCrMo	COCr	XLPE	762.05	10.02
DP12	COCr	Ti30Nb5Sn5Zr	Polyurethane	→ 677.91	9.95
DP13	COCr	Ti6Al4V	HDPE	738.17	9.96
DP14	COCr	CoCrMo	XLPE	759.77	9.97
DP15	COCr	COCr	UHMWPE	699.61	→ 9.89

Hosseinzadeh et al. (2012) reported that –even though there are wear problems with UHMWPE- the CoCr-UHMWPE pair is very widely used as a bearing material combination for the hip joint [8]. In another study conducted by Kalayarasan et. al. (2013), it was demonstrated that within four different material combinations for total hip prostheses, the CoCr-UHMWPE combination had the potential to extend the life of the implant compared to other material combinations. When the results of the current study are carefully examined, it is seen that the results are consistent with the previous studies. However, there are some limitations in this work. The bone model, obtained as a single segment, needs to be acquired in segments representing trabecular and cortical bone. Moreover, the effects of muscle forces may be considered for a more realistic simulation.

CONCLUSIONS

According to the results of the study, it is assessed that for the maximum stress obtained on the implant, the material combination of CoCr-Ti30Nb5Sn5Zr-Polyurethane for the hip implant, acetabular cup, and plastic liner, respectively, could be appropriate, and for the maximum total deformation observed in the implant, the selection of the CoCr-CoCr-UHMWPE combination may be a better alternative.

REFERENCES

[1] A. B. Batıbay, “Mekanik alaşımlama yöntemi ile üretilen ti-nb esaslı alaşımların mikroyapısal, mekanik, antibakteriyel ve sitotoksik özelliklerinin incelenmesi”, 2021.

[2] E. Bahçe, A. K. Aslan, M. S. Güler, N. Çakir, ve E. Emir, “Kalça Protezinin Aşınma Özellikleri Üzerinde Çoklu Tabakalı Kaplanmasının Etkilerinin Sonlu Elemanlar Metoduyla Nümerik Analizi”, Ordu Üniversitesi Bilim Ve Teknol. Derg., c. 7, sy 2- 2, 2017.

[3] S. M. S. Toh, A. Ashkanfar, R. English, G. Rothwell, D. J. Langton, ve T. J. Joyce, “How does bicycling affect the longevity of Total Hip Arthroplasty? A finite element wear analysis”, J. Mech. Behav. Biomed. Mater., c. 139, s. 105673, 2023.

[4] M. Kalayarasan, L. Prakash, ve S. Shankar, “Material selection of acetabular component in human hip prosthesis using finite element concepts”, Int. J. Exp. Comput. Biomech., c. 2, sy 2, ss. 118-135, 2013.

[5] M. Dumas, P. Terriault, ve V. Brailovski, “Modelling and characterization of a porosity graded lattice structure for additively manufactured biomaterials”, Mater. Des., c. 121, ss. 383-392, May. 2017.

[6] Free CAD designs, Files; 3D models: The grabcad community library, https://grabcad.com/library/distal-femur-2

[7] Free CAD designs, Files; 3D models: The grabcad community library, https://grabcad.com/library/hip-prosthesis-2

[8] Hosseinzadeh, H. R. S., Eajazi, A., & Shahi, A. S., “The bearing surfaces in total hip arthroplasty–options, material characteristics and selection”, Recent advances in arthroplasty, 163-210, 2012.

LEAN MASS AND ISOMETRIC UPPER BODY STRENGTH ARE ASSOCIATED WITH SPRINT KAYAK PERFORMANCE

Mathias Kristiansen[1], Matthew Flood[1] and Kent Klitgaard[1]

[1]ExerciseTech, Department of Health Science and Technology, Aalborg University, Aalborg, Denmark

INTRODUCTION

Flat water sprint kayak performance is largely determined by the work capacity of the upper body musculature. As such, we have previously shown a relationship between maximal dynamic strength in the bench press and performance in 200 m sprint kayak [1]. Similarly, other studies have shown that a relationship exists between anthropometry, strength, body composition, and short-distance sprint kayak performance [2,3]. This seems to indicate that distances that have a high contribution from the anaerobic energy system depend upon both strength and lean body mass. However, it remains unclear whether upper body strength levels and body composition are associated with distances where the aerobic energy system is predominant. Therefore, the aim of the present study was to investigate the relationship between upper strengh measured using a kayak specific isometric dynamometer and lean mass with either maximal power output or 2000 m kayak performance.

METHODS

Fifteen elite kayak paddlers (11 males and 4 females) visited the laboratory for one testing session. First, body composition was assessed using a dual energy x-ray absorptiometry (DEXA) scanner. Lean mass was extracted from the measurements of the arms, legs, trunk and full body, respectively.

Next, maximal force in the middle of the stroke phase was recorded using a custom-made setup. The setup comprised a Dansprint single-arm kayak machine attached to a cable pulley via a chain. A force transducer was mounted between the chain and the single-arm machine, with a sampling frequency of 1000Hz. The cable pulley was locked during the test, and an isometric voluntary contraction was performed. Two trials were performed with 1-minute rest in between.

Lastly, a 5 s maximal power test and a 2000 m time trial was performed on a kayak ergometer. Before testing, all subjects completed a 10 min warm-up. Pearson product moment correlation analysis was performed to determine the relationship between force output in the single arm machine and lean body mass and the two kayak-specific tests of maximal power and 2000 m performance time.

RESULTS AND DISCUSSION

The force output obtained in the single arm machine was positively correlated with the maximal power output obtained on the kayak ergometer ($r = 0.78$, $p \leq 0.001$). Similarly, force output was negatively correlated with 2000 m performance time ($r = -0.53$, $p = 0.042$).

Lean mass of the arms, legs, trunk, and full body were all positively correlated with maximal power output obtained on the kayak ergometer ($r \geq 0.69$, $p \leq 0.05$). Similarly, the lean mass of the arms, trunk and full body were all negatively correlated with 2000 m performance time ($r \geq -0.60$, $p \leq 0.05$). These results indicate that kayak specific strength and the amount of lean mass possessed by a highly trained elite kayak paddler are closely related to the ability to generate maximal power in a 5 s test on a kayak ergometer. Moreover, that lean mass and strength, except for the lean mass of the legs, is also related to the predominantly aerobic performance of the 2000 m kayak ergometer test.

More muscle mass and the ability to exert higher forces through the paddle during kayaking may explain the relationship between these physical attributes and longer distance kayak performance. Further, as kayaking is not a weight bearing event, the energetic cost of moving a larger body mass in the kayak is trivial, compared to the increased work capacity of the extra added muscle mass.

CONCLUSIONS

Isometric force output and lean mass are closely associated with maximal power output and 2000 m performance on a kayak ergometer in highly trained elite kayak paddlers.

REFERENCES

1. Kristiansen M, et al. J Strength and Cond Res. 37,4, e305-e312. 2023
2. van Someren KA, et al. Int J Sports Physiol Perform. 3, 207-218. 2008
3. Akca F. Int J Appl Sports Sci. 20, 1, 22-30. 2008

Table 1 Correlation coefficients describing the relationship between lean mass (LM), force output in the single arm kayak machine, maximal power output and 2000 m kayak performance time. * = $p \geq 0.05$

	Power	Time (2000 m)	LM (Arms)	LM (Legs)	LM (Trunk)	LM (Full body)	Force
Power	1						
Time (2000 m)	-0.47	1					
LM (Arms)	0.88*	-0.60*	1				
LM (Legs)	0.70*	-0.35	0.86*	1			
LM (Trunk)	0.69*	-0.73*	0.90*	0.81*	1		
LM (Full body)	0.76*	-0.60*	0.95*	0.93*	0.96*	1	
Force	0.78	-0.53*	0.74*	0.61*	0.74*	0.73*	1

PATIENT-SPECIFIC SPINAL BONE SCREW FIXATION: HOMOGENIZED VERSUS VOXEL-BASED FINITE ELEMENT ANALYSIS

Mohammadjavad Einafshar[1,*] Alireza Rouyin[2], Mohadese Rajairad[3], Mohammadjavad Salmani[2], Farzam Farahmand[2], Navid Arjmand[2]

1. Department of Material and Production, Aalborg University, Aalborg, Denmark
2. Department of Mechanical Engineering, Sharif University of Technology, Tehran, Iran
3. Department of Biomedical Engineering, university of Isfahan, Isfahan, Iran

INTRODUCTION

Bone screws are vital for orthopedic procedures but often lead to issues like dislocation and bone problems. Current testing with cadaver bones is slow and lacks consistency [1,2]. Computer simulations provide a faster, cost-effective way to assess screw designs and reduce the need for human samples. Numerical models consider factors like geometry and materials but struggle with bone variability [3]. Micro finite element analysis shows promise but needs to accurately represent non-linear effects and the bone-screw interface. Few studies have compared numerical models to mechanical tests, especially concerning stiffness and strength [4]. This study aims to quantify pull-out characteristics of bone screw in both homogenized and non-homogenized material.

METHODS

The finite element (FE) model was created using CT images of two 23–26-year-old volunteers without a history of low back disease. The bone segmentation was performed using Mimics software, and posterior elements were removed with 3-Matic software (Fig. 1.A). Each vertebra had a 30 mm long, 5.5 mm diameter, and 2.5 mm pitch screw inserted with a 0.05 mm gap. The screw paths followed the oblique lumbar interbody fusion (OLIF) approach. Material properties were assigned to each vertebra based on voxel-based or homogeneous modeling. Voxel-based modeling considered material heterogeneity, while homogeneous modeling used the average Hounsfield value of a two-fold-diameter of the screw as the material reference volume (Fig. 1.C). Relationships were used to convert Hounsfield values to mechanical properties. Cortical bone voxels with Hounsfield values greater than 500 HU were modeled homogeneously. The thin shell of the vertebral body had a negligible impact on results. Interface modeling employed a general contact model with a tangential friction coefficient of 0.2 and hard contact conditions between screw threads and the threaded hole in the vertebra. Boundary conditions involved clamps at the anterior and posterior shell of the vertebral body (Fig. 1.B). A 0.25-mm displacement along the screw's longitudinal direction simulated pull-out.

RESULTS AND DISCUSSION

A total of 20 pull-out tests were simulated using and the obtained pull-out forces ranged from 652 to 1424 newtons. The pull-out displacement ranging from 0.188 to 0.21 mm. The pull-out stiffness varied from 6792 to 14402 N/mm (Table 2), and the pull-out strain energy ranged from 58 to 91 N.mm (Table 4). Furthermore, the stress contour was shown in three states: the first simulation, maximum force, and after damage (Table 1). The relationships between the forces and the stiffnesses and their errors in the two cases of voxel-based and homogeneous in the different standard deviations of material reference volume are reported in the graphs.

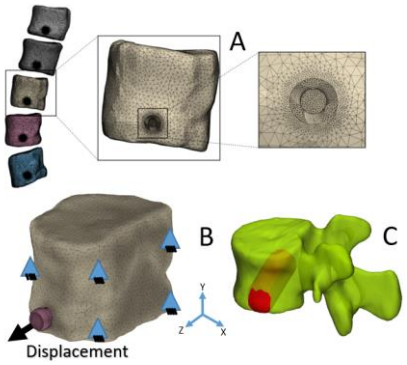

Fig. 1. A) 3D model fabrication, B) Boundary Conditions and C) two-fold-diameter material reference volume.

CONCLUSIONS

The present study introduces a novel methodology for conducting investigations on cancellous bone with homogenous modeling. Prior to this research, the only viable approach was to employ heterogenous models. By leveraging the findings of this study, it is now feasible to replicate the authentic conditions of cancellous bone in a patient-specific pull-out test on a block.

Table 1. Voxel-based and homogenous force calculation. The Force errors were also calculated between two models.

Vertebra	Hu	Force (N)		Error (%)
		Voxel-based	Homogenous	
L1	84	952.8	977	9.7
L2	88	990.3	1021.8	4.3
L3	88	1065.2	1041.6	3.8
L4	125	1305.9	1070.8	10.1
L5	105	1165.7	1049.6	16.4
L1	58	994.9	1257.4	21.8
L2	57	1391.4	1401.8	4.8
L3	61	1408.9	1424.3	9.1
L4	63	1155.1	1224.7	5.4
L5	76	1155.2	1269.8	6.7

REFERENCES

[1] Einafshar, M et al. *J Arch Bone Jt Surg*, **10**: 204-212,2022.
[2] Einafshar, M. et al. *J Med Biol Eng*, **41:** 447–455, 2021.
[3] Einafshar, M. et al. *JOR spine*, **e1220**, 2022.
[4] Einafshar, M. et al. *J Comput Methods Programs Biomed*, **202:** 105966,2021.

A PRELIMINARY ANALYSIS ON THE FEASIBILITY OF DETECTING GAIT EVENTS USING MACHINE LEARNING AND MOTION SENSORS EMBEDDED IN SMARTPHONES

Larsen, Aske G.[1], Sadolin, Line Ø.[1], Thomsen, Trine R.[1], Oliveira, Anderson S.[2]

Aalborg University, Department of Chemistry and Bioscience[1], Aalborg University, Department of Materials and Production[2]

INTRODUCTION

Smartphones have garnered attention as wearables within Human Activity Recognition (HAR) due to their low cost and high accessibility. Current smartphones are equipped with motion detection sensors such as accelerometers, gyroscopes, and magnetometers, which are used in various applications including navigation, gaming, and fitness monitoring. Motion sensors have been extensively used in Har, towards developing methods capable of automatically identifying and categorizing human actions [1]. The literature has shown the potential of using smartphones in HAR, especially for gait analysis [2]. However, people walk at different speeds and carry their smartphones at different locations (trousers, jackets, etc), and there are no algorithms dedicated to flexibly identifying gait events from motion data regardless of the phone location and walking speed. Therefore, the aim of this study was to create a robust machine learning algorithm that can accurately predict gait events regardless of the position of the phone and walking speed.

METHODS

20 males and 6 females (age: 36.4±18.2 years, height: 176.4±20.2 cm, body mass: 86.8±15.7 kg) participated in the study. Participants were instructed to walk on a treadmill at 1 m/s, 1.25 m/s and 1.5 m/s for 110, 90 and 80 seconds respectively. The task was repeated 3 times, since participants were asked to carry a mock phone in the right pocket of a jacket, the right front pocket of their trousers or in the right hand. The mock phone contained an embedded Inertial Measurement Unit (IMU) (Trigno Avanti Sensor, Delsys Inc., Massachusetts, USA) for the acquisition of 3D accelerations and angular data. The ground truth initial contact and toe-off events (timestamps) were defined from optical motion capture, by fitting retro-reflective optical markers on the calcaneus and tip of the first metatarsal bilaterally. Both IMU and marker data were synchronized.

A machine learning algorithm dedicated to classify 3D accelerations and angular rates time series as ”heel strike”, ”toe-off” or ”not-event” was created using a combination of a Convolutional Neural Network (CNN) and bidirectional long short-term memory neural network (LSTM) architecture. The CNN-LSTM comprised of 2 CNN layers, a single bidirectional LSTM layers and 2 dense neural layers, each utilizing the Leaky rectified linear unit (ReLU) activation function, except for the final output layer, which employed the activation function Hyperbolic Tangent Function (Tanh). In total 6337 complete gait cycles were used. The data was divided into 200 ms windows, with 95 % overlap, which were then split 80/20 into training/testing data. All data were normalized using a Robust Scaler algorithm. We reported the overall accuracy in predicting the time series windows containing the events of interest (heel strike, toe-off), as well as the mean error (in ms) to define the exact instant of gait events..

RESULTS AND DISCUSSION

In general, we succeeded in defining gait events with an average accuracy of 87% (range: 81%-96%, Table 1). The mean error in defining the instant of gait events was 73±102 ms, which corresponds to ~4.8% average gait cycle duration. Previous studies investigating similar topics have shown greater performance with F1-Measures (≥94%) [3]. However, the authors used inputs from four different IMUs placed on the shank and above the ankle joints bilaterally. Therefore, the accuracy from our study using only one IMU is promising, since there was no strict fixation of the mock phone nor any control of the clothing people used.

CONCLUSIONS

Our preliminary analysis demonstrated that CNN-LSTM retrieves bilateral gait events with high accuracy (~87%) despite the different phone locations and walking speeds. Further validation including more participants are likely to increase the current accuracy. These results demonstrate the potential of using machine learning to perform remote gait analysis on mass scale using smartphone motion sensors.

REFERENCES

1. Ann, O. C., & Theng, L. B. (2014, November). Human activity recognition: A review. In *2014 IEEE international conference on control system, computing and engineering (ICCSCE 2014)* (pp. 389-393). IEEE.
2. Straczkiewicz, M., James, P., & Onnela, J. P. (2021). A systematic review of smartphone-based human activity recognition methods for health research. *NPJ Digital Medicine*, *4*(1), 148.
3. Romijnders, R., Warmerdam, E., Hansen, C., Schmidt, G., & Maetzler, W. (2022). A deep learning approach for gait event detection from a single shank-worn imu: Validation in healthy and neurological cohorts. *Sensors*, *22*(10),

Table 1. Prediction accuracies for heel strike (HS) and toe-off (TO) events for the combination of the three phone placements and three gait speeds.

	Hand			Jacket Pocket			Trouser pocket		
	3.5 km/h	4.5 km/h	5.5 km/h	3.5 km/h	4.5 km/h	5.5 km/h	3.5 km/h	4.5 km/h	5.5 km/h
Left HS	0.88	0.84	0.88	0.89	0.84	0.85	0.91	0.86	0.81
Right HS	0.93	0.94	0.95	0.88	0.84	0.90	0.94	0.96	0.95
Left TO	0.86	0.83	0.87	0.84	0.82	0.81	0.90	0.85	0.87
Right TO	0.89	0.87	0.90	0.84	0.85	0.87	0.92	0.89	0.82

CHILDREN DIAGNOSED WITH IDIOPATHIC TOE WALKING – ALTERED TREATMENT STRATEGY WHEN 3D-GAIT ANALYSIS IS ADDED TO THE DECISION-MAKING

Anders Holsgaard-Larsen (ahlarsen@health.sdu.dk)[1-2], Tina Udemark Pasgaard[1], Sidsel Hald Rahlf[1], Julie Ladeby Erichsen[1], Bjarke Viberg[1-2], Christian Færgemann[1]

[1] Department of Orthopaedics and Traumatology, Odense University Hospital, [2] Department of Clinical Resaerch, Orthopaedic Research Unit, University of Southern Denmark

INTRODUCTION

Idiopatic toe walking (ITW) is a diagnosis for children walking on their toes with no medical cause [1] and is a common pattern seen in healthy children less than 3 years old [2]. Consequences of ITA include ankle/foot pain, poor function/performance, and stigmatization plus parental concern. Orthopaedic treatment strategies for children diagnosed with ITW after the age of approximately 5 years typically include serial casting or achilles lengthening surgery intending to reduce ankle equinus. Determining, the cause and the severity of ITW and the associated treatment may be difficult from clinical examination alone. 3D-Gait analysis might provide a further objective and quantitative description of ITW potentially altering the treatment strategy.

Aim: To test the hypothesis that the treatment strategy of children diagnosed with ITW from a clinical examination and considered candidates for achilles lengthening surgery based upon ankle equinus would change once objective and quantitative information from a 3D-gait analysis were added.

METHODS

This is a cross-sectional analysis on baseline data from a prospective cohort (powered for another research question). Inclusion: Children (7-15 years) referred to the pediatric orthopedic outpatient clinic at Odense University Hospital or Kolding Hospital and considered candidates for surgical treatment for ITW based upon a) parent reported toe-walking, b) visual signs of toe-walking, and c) passive ankle dorsiflexion <15˚ with the knee extended. Exclusion: Children with neurological conditions, unilateral toe-walking, previous Achilles lengthening surgery, club foot, and not understanding Danish.

Following clinical ITW examination at the outpatient clinic, children were referred to a confirmatory 3D-Gait analysis. Children walked barefooted at a 10-meter walkway at self-selected speed. Kinematic and kinetic variables were captured via an 8-camera 3-dimensional marker-based motion analysis system (Vicon, T40, Oxford, England). The standard plug-in-gait marker-set was applied and corresponding analysis on kinematic and kinetic variables were performed in Nexus 2.12. Based upon waveforms of the ankle kinematics and kinetics children were subsequently dichotomized according to Alveraz et al 2007 into; 1) no – mild signs or 2) moderate – severe signs of ITW [3].

RESULTS AND DISCUSSION

23 children (17% girls, age 10 ± 2 years (mean ± sd)) were included in the study. Using the categories by Alveraz et al 2007 [3], 13 children showed moderate - severe signs of ITW whereas, 10 children showed no - mild signs of ITW and thus, not considered candidates for Achilles lengthening surgery. Differences in dynamic ankle function between the two groups were observed for peak ankle dorsi-flexor degree during stance (4.5 ± 5.8˚ vs 13.4 ± 1.4˚, $p < 0.001$), ankle plantar flexion at initial contact (12.3 ± 7.8˚ vs 2.5 ± 3.0˚, $p < 0.001$), and delta of the two peak ankle plantar-flexer moments (0.09 ± 0.29 Nm/BW vs 0.68 ± 0.19 Nm/BW, $p < 0.001$) (indicating equinus). However, no differences were observed in knee kinematics or kinetics (Table 1).

CONCLUSIONS

Adding objective and quantitative information from a 3D-Gait analysis to the decision making of ITW altered the treatment strategy for almost half of the children considered to be candidates for Achilles lengthening surgery. From a clinical perspective this raises the question whether we are treating/operating too many children where the underlying cause of toe walking is not identified.

REFERENCES

1. Sala DA, et al., *Dev Med Child Neurol* **41**: 846-8, 1999
2. Caserta A, et al., *Gait & Posture* **67**: 181-6, 2019
3. Alverez C, et al., *Gait & Posture* **26**: 428-35, 2007

Table 1. Kinematic and Kinetic values for the Moderat-Severe ITW and No-Mild ITW Groups.

		Group Moderat / Severe Mean ± SD	Group No / Mild Mean ± SD	p-value
Peak Dorsal Flexion Angle (Stance)	[Degree]	4.47 ± 5.82	13.41 ± 1.38	< 0.0001
Ankle angle (Initial Contact)	[Degree]	12.28 ± 7.82	2.54 ± 3.03	< 0.0001
Minimum Knee angle (Mid Stance)	[Degree]	0.767 ± 4.63	2.25 ± 4.79	0.31
Δ Ankle Moment (Loading Respons vs Mid Stance)	[Nm / Kg]	0.09 ± 0.29	0.68 ± 0.19	< 0.0001
Peak Knee Extension Moment (Mid Stance)	[Nm / Kg]	0.32 ± 0.17	0.26 ± 0.16	0.18

BIOMECHANICAL EFFICACIES OF STABILIZATION OF LUMBAR DEGENERATIVE DISEASES USING HYBRID INSTRUMENATIONS: A FINITE ELEMENT STUDY

Moustafa Mesbah [1,2,*], [1]Mohamed Bendoukha, [3]Abdelwahed Berkaoui, [4]Hakim Chiali

[1]Department of Mechanical Engineering, University of Mostaganem, Algeria
[2]Department of Materials and Production, Aalborg University, Denmark
[3] College of Engineering and Architecture, International University of Rabat , Morocco
[4]Radiology and Medical Imaging Department, Tlemcen University Hospital. Algeria

INTRODUCTION

Pedicle-based hybrid stabilization (PBHS) has been suggested to treat degenerative disc disease (DDD) and avoid adjacent segment disease (ASD) by establishing a smoother transition from instrumented segments to adjacent untreated levels. However, its biomechanical efficacies are unclear, and problems associated with them need to be elucidated [1, 2]. In this study, a finite element (FE) study was performed to assess the biomechanical efficacies of some of the currently available PBHS stabilizations on the biomechanical behavior of the lumbar spine by assessing range of motion (ROM) and peak loads over the lumbar segments and the instrumentations.

METHODS

A 3D muscular ligamentous L2-S1 FE-Model validated based on in vivo data was used in this study [1]. The FE-model was adapted to simulate the post-op changes to simulate the L3-L5 level instability by nucleotomy at L4-L5. The instrumented models were further made by modifying the intact model to simulate the implantation of hybrid constructs at L3-L4 and L4-L5 (Figure 1). The FE-model allowed mimicking the surgical approach by placing the anterior lumbar interior fusion (ALIF) cage within the intervertebral disc space [2, 3]. The model was subjected to combined loading. 10 Nm + 400 N was applied to the intact and instrumented models while under follower muscular loads. Flexion, extension, axial rotation, and lateral bending were conducted to measure the ROM and peak von Mises stress (PVMS) over the instrumentations. The likelihood of failure at the rods was evaluated by the ratio between the PVMS and yield strength of each rod.

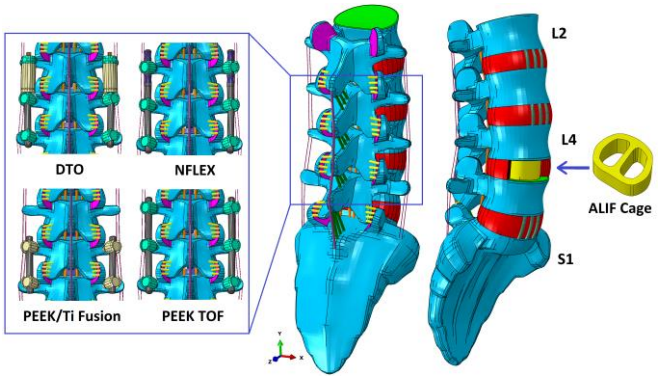

Fig. 1 FE-Models of instrumentation with PBHS systems.

RESULTS AND DISCUSSION

The segmental ROM in flexion, extension, lateral bending and axial rotation for stabilization with a hybrid constructs expressed relative to the intact spine is shown in Figure 2.
The segmental ROM in flexion, extension, lateral bending, and axial rotation for stabilization with a non-fusion system expressed relative to the intact spine is shown in Figure 2. After the application of a PBHS, changes occurred in the lordotic angle as compared to the intact model. The PBHS rods increased the ROM in all motions compared to the intact model (5~53%). The titanium and PEEK rods induced increased motion at the adjacent segment L3-L4 (55%~115%), and at the fused segment L4-L5, all implants had the same stabilizing effect and reduced the angular motion by 36~56%. The PBHS systems are highly stressed, especially the DTO and NFlex systems, while the rest of the structure's motion is preserved (Figure 2). Loads in the flexible PEEK topping-off fusion (TOF) are all lower than in the DTO and NFlex systems. Therefore, this stress distribution may reduce the possibility of broken rods. The PEEK rod may result less stiff instrumentations and less von Mises stress on rods compared with rigid fusion fixators.

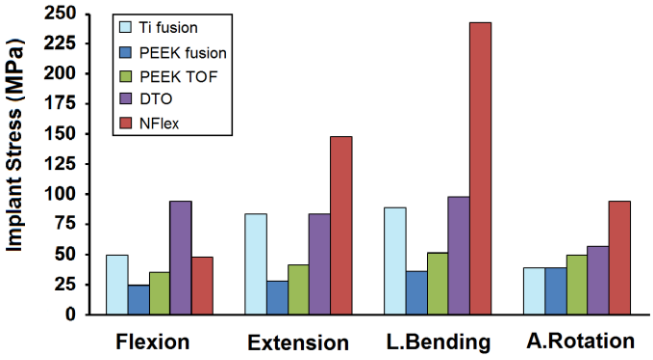

Fig.2 PVM stress over different types of instrumentation

CONCLUSIONS

PBHS can decrease the ROM of the upper adjacent segment and slightly increase the ROM of other segments, thereby delaying the degeneration of upper adjacent segments and compensating for lumbar spine mobility. The hybrid stabilization offers particular protection against fusion-induced ASD and its adverse effects. PEEK TOF may reduce the possibility of broken rods.

REFERENCES

1. Mesbah M et al. Series on Biomechanics. **33**: 27– 39, 2019
2. Mesbah M & Barkaoui, A. Traumatol Surg Res. **107**:1030-1038, 2021
3. Mesbah M & Barkaoui A. Proc Inst Mech Eng H. **234**: 931-941, 2020

PREDICTION OF DISCRETE FOOTBALL ACTIONS USING SEMI-SUPERVISED MACHINE LEARNING

Department of Health Science and Technology, Aalborg University [1]
Department of Materials and Production, Aalborg University [2]
Larsen, Aske Gye*[1], Papi, Giovanni*[1] & Oliveira, Anderson Souza[2]
*Student

INTRODUCTION

The popularity of wearables in football is on the rise, yet their full potential remains largely untapped [1]. In particular, the current use of Inertial Measurement Units (IMUs) primarily focuses on measuring workload and running patterns, with recent advancements enabling the prediction of precise movements such as shots or sprints using machine learning [2,3].

However, predictions of football actions with similar motion patterns such as dribbling, first touches, positioning and passing are scarce in the literature. Therefore, this study aims to test if the integration of IMUs with established principles of machine learning reliably can predict football actions with common movement patterns.

METHODS

In this study 14 male and 3 female (age: 19.1±6.9 years old, height: 174.5±10.3 cm, body mass: 62.4±23.1 kg, football experience: 9.7±3.6 years) football players participated. The participants engaged in various passing and dribbling drills using a goal station setup (Goal Station Focus 360, Goal Station ApS, Aalborg, Denmark). In total 196 trials were recorded (11.53 ± 4.53 per participant & 44.87 ± 16.93 minutes per participant). Video was recorded using a semi-professional camera (Nikon 1 J4, Nikon Company, Tokyo, Japan) at 60 frames per second. The video was used to label the data collected using the Xsens Awinda (Xsens MVN Awinda, Xsens Technologies B.V, Enschede, the Netherlands) from 7 IMUs at 60 Hz placed on the head, sternum, right wrist, right calf, left calf, right foot and left foot. The 3D-accelerometer, 3D-gyroscope, 3D magnetometer and 4D quaternion were all included, and furthermore the magnitude and derivatives of the signal was calculated. A total of 5250 statistical time domain features were calculated over a sliding window of 200 ms, with 50 % overlap, but later reduced to 948 principal components utilizing a Principal Component Analysis retaining >95 % of the variance. A semi-supervised uncertainty-aware pseudo-labeling technique was used to decrease the time needed for labeling. The data were trained using a bidirectional long short-term memory neural network (bi-LSTM) architecture. The bi-LSTM comprised 2 bidirectional LSTM layers and 4 dense neural layers, each utilizing the parametric rectified linear unit (ReLU) activation function, except for the final output layer, which employed the softmax activation function. A dropout of 0.4 was applied to all hidden layers and the input layer. An early stop mechanism with a limit of 35 epochs was implemented to prevent overfitting. Focal categorical cross-entropy was chosen as the loss function, and the Adam optimiser was employed. A soft voting sliding window post-processing technique was applied, with 50% weight assigned to the current window and 25% weight each to the preceding and subsequent windows, respectively.

RESULTS AND DISCUSSION

The performance of the bi-LSTM model's predictions for various football actions is depicted in Figure 1 through a confusion matrix. Notably, the algorithm demonstrated higher accuracy in predicting positioning and passing actions, while encountering challenges in accurately predicting first touch and dribbling actions. The observed accuracies were notably lower than those reported by Cuperman et al. in 2022 and Schuldhaus et al. in 2015, both of which achieved accuracies exceeding 80%. It is essential to consider that their experiments were conducted in a more controlled environment, and they also encountered reduced accuracies when dealing with similar movement types [2,3].

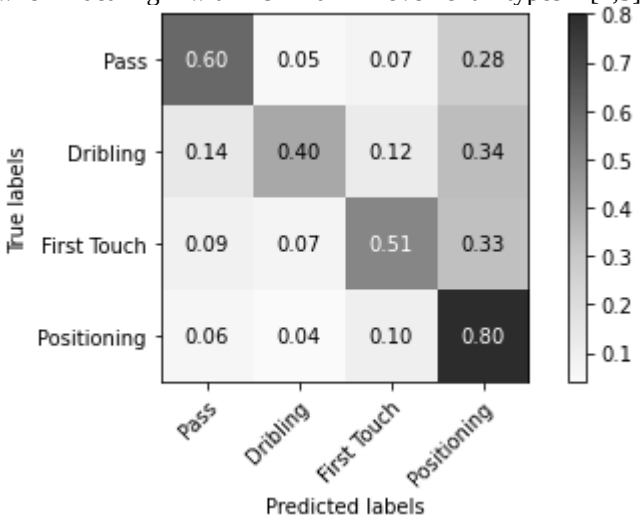

Fig. 1 A normalized confusion matrix of the bi-LSTM, with predicted events on the x-axis, and actual events on the y-axis. The hue indicates the share of the prediction.

CONCLUSION

Our study demonstrated a reasonable prediction accuracy of overlapping football actions by using IMUs and bi-LSTM neural networks. However, the accuracy is considerably lower compared to earlier more controlled studies, indicating the need for more data.

REFERENCES

1. Cust, E. E., Sweeting, A. J., Ball, K., & Robertson, S. (2019). Machine and deep learning for sport-specific movement recognition: A systematic review of model development and performance. *Journal of sports sciences*, *37*(5), 568-600.
2. Cuperman, R., Jansen, K. M. & Ciszewski, M. G. (2022), 'An end-to-end deep learning pipeline for football activity recognition based on wearable acceleration sensors'
3. Schuldhaus, D., Zwick, C., Körger, H., Dorschky, E., Kirk, R. & Eskofier, B. M. (2015), Inertial sensor-based approach for shot/pass classification during a soccer match, in 'KDD workshop on large-scale sports analytics

Kinematic analysis of the two phases, jump on trampette and trampette support phase, with focus on angles and angular velocity in the lower body.

Østerballe, Nielsen, W. Nielsen & K. Nielsen, hst-23-idr-7-7104@student.aau.dk
Aalborg University
Knee angle[5], Hip angle[5], Flight time[1], Tucked Barani Out[2], Vaulting[2], Gymnast

Introduction

This study is an explorative study that aimed to examine the potential effects of two phases, jump on trampette and trampette support phase, on the flight time. Where the focus in these phases was on knee and hip angle for the swing and takeoff leg, and average hip angular velocity for the takeoff leg. This was based on the need for better understanding the two phases [2,3].

Method

This study included eight elite gymnasts (age: 24 ± 2,2, weight: 72,8 ± 6,7 kg, height: 178,4 ± 5,2 cm) where each participant performed five tucked barani out (TBO), resulting in 36 correct performed TBO. A TBO can be divided into five phases: 1) running phase, 2) jump on trampette phase, 3) trampette support phase, 4) flight phase and 5) landing phase [1]. Each performance was measured using Xsens MVN Link Lycra Suit with 17 IMUs and were analysed using Xsens MVN Analysing tool (MVN Analyze 2023.0, Technologies B.V., the Netherlands; Enschede) [5]. Hip and knee angles for both takeoff (TL) and swing leg (SL) in phases two and three were found for all participants. The predetermined point in time for the jump on trampette phase was when the hip angle of TL was at its lowest and the predetermined point in time for the trampette support phase was when the hip angle of TL was at its highest (fig. 1). The average angular velocity was found by using the time from phase two to phase three divided by angle differences for the hip. Flight time for each performance was also found.

Results and discussion

The results of this study showed low to no positive or negative correlation with the following parameters and flight time: Knee and hip angle for SL and TL in either of the phases, and average hip angular velocity for TL [Table 1]. Results do show a relatively similar flight time for all participants TBO [Figure 1]. Bjørn states that specific positions are very important for the optimal outcome in a TBO and vaulting in general [2]. Whereas Jemni [4] argues that different vaulting exercises depends on the complexity of the jump, where there are different work requirements for all gymnasts because of different body compositions.
Based on these studies [2,4] and this explorative study, it can be deduced that different workouts and vaulting techniques can have an influence on angular velocity, hip and knee angle in vaulting, when performing TBO.

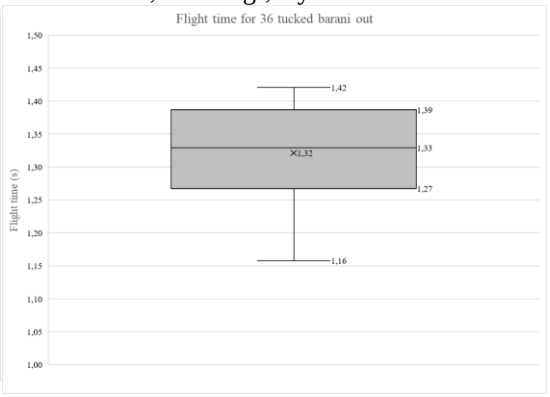

Fig. 1: Flight time with minimum value, maximum value, first quartile (Q1), third quartile (Q3), median and mean value (X) of the 36 correct tucked barani out.

Conclusion

This study concluded that the jump on trampette phase and trampette support phase cannot explain alone how the flight time is affected and more research is needed to explain this. Because of deviating hip and knee angles between participants and between individual trials, despite the relative same flight time.

Acknowledgement

PE-Redskaber A/S, Denmark, Gram.

References

1. A. Atikovic et al., *Effects of a mini-trampoline exercise during 15 weeks for increasing the vertical jump performance*, **15**, p. 11–19, 2018.
2. J. Barreto et al., *How Task Constraints Influence the Gaze and Motor Behaviours of Elite-Level Gymnasts*, **18**, no. 13, p. 6941, 2021.
3. Bjørn, M. *Bogen om springgymnastik* 1st ed. Vejle, 1994.
4. M. Jemni, *The Science of Gymnastics*, 2nd ed. Milton: Routledge, p. 45–48 & 82, 2018.
5. Roetenberg, D., Luinge, H., & Slycke, P. *Xsens MVN: Full 6DOF human motion tracking using miniature inertial sensors*. Xsens Technologies, **3,** p. 1-9, 2013.

Table 1: Calculated Pearson Correlation for flight time with the measured parameters. The parameters are numbered as following: a) Hip angle of TL in phase 2, b) Hip angle of SL in phase 2, c) Knee angle of TL leg in phase 2, d) Knee angle of SL in phase 2, e) Hip angle of TL in phase 3, f) Hip angle of SL in phase 3, g) Knee angle of TL in phase 3, h) Knee angle of SL in phase 3 and i) Angular velocity.

	Pearson Correlation with the measured parameters and flight time								
	a	**b**	**c**	**d**	**e**	**f**	**g**	**h**	**i**
R-value	0,021	-0,107	0,052	0,166	0,347	0,412	-0,221	0,011	0,338
p-value	0,904	0,534	0,765	0,333	0,038	0,013	0,196	0,951	0,032

Evaluation of trip-reducing elements using a mechanical free body shoe collision test

Mathias Munk-Hansen[1], Anders Holsgaard-Larsen[2], Mark de Zee[1], Thor Grønlykke[3], Pascal Madeleine[1]
[1] ExerciseTech, Department of Health Science and Technology Aalborg University, Aalborg, Denmark
[2] Department of Orthopaedics and Traumatology, Odense University Hospital and Department of Clinical Research, University of Southern Denmark, Odense, Denmark
[3] Spraino ApS, Copenhagen, Denmark

INTRODUCTION

Trips at workplaces are safety hazards that have important personal and socio-economic consequences [1]. Trips can happen over small perturbations as low as five mm [1,2] making it almost impossible to provide effective safety regulations in occupational settings. A Danish company (Spraino ApS) focuses on lowering the risk of injury due to tripping. This is done by mounting low friction and angle modifying elements called "TripStop" on the toecap of a safety shoe. For further development of the TripStop, it is important to quantify the mechanical effect of these shoe modifications. The aim of this study was to develop a mechanical test method for testing how the mechanical breaking properties of a safety shoe are affected when colliding against a perturbation and whether toecap modifications can alter these.

METHODS

The modified safety shoe was tested against the same type and size of safety shoe without any modifications (Noseslide, TOWORKFOR, Guimarães, Portugal). The collision test was adapted from a setup described by Fong et al. [3], using a pulley system as an actuator to pull a shoe across a force plate, allowing the extraction of the friction between the shoe and the floor. An obstruction bar was fixed to a force plate (model OR6-5-2000, © Advanced Mechanical Technology, Inc., Watertown, MA, USA) and the safety shoe was placed on a sled in a track to control the collision (Figure 1). Motion capture data (Qualisys Track Manager, 2022.1, Göteborg, Sweden) of the shoe was collected with a reflective marker placed on the top of the toecap of the shoe.

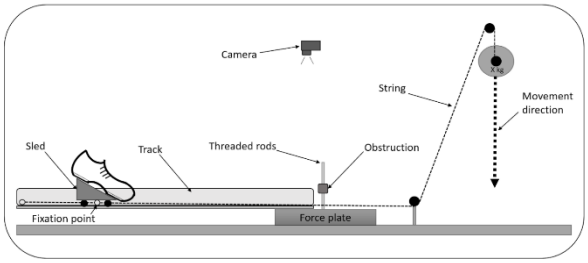

Figure. 1 Experimental setup.

The string attaching the pulley system to the sled was placed under the obstruction bar to minimize interference with the force plate. Furthermore, another string was mounted at the back of the track to stop the displacement of the sled avoiding collision with the obstruction bar. The acceleration started from a fixed point resulting in the shoe having the same momentum at initial contact with the obstruction bar. Ten trials were made for both shoe conditions. A paired t-test was performed to compare peak horizontal braking force and impulse of the horizontal braking force for the first 20 ms after initial contact.

RESULTS AND DISCUSSION

The peak braking force was significantly lower for the modified shoe (62±66 N) compared with the control shoe (367±21 N, $T(18)=13.97$, $P<0.001$). The braking impulse was also lower for the modified shoe (13.8±11.9 Ns) compared with the control shoe (94.9±3.3 Ns, $T(18)=20.83$, $P<0.001$). Consistent force-time curves over the 10 trials for both the control shoe and the modified shoe were observed (Figure 2). Besides altering the braking force, the modification changed the horizontal and vertical movement of the shoe after the collision. The control shoe was initially pushed back before it moved over the obstruction bar. This means that the shoe rotated around the obstruction bar. On the contrary, the modified shoe was lifted and kept moving forward, which could be beneficial in recovering from a trip.

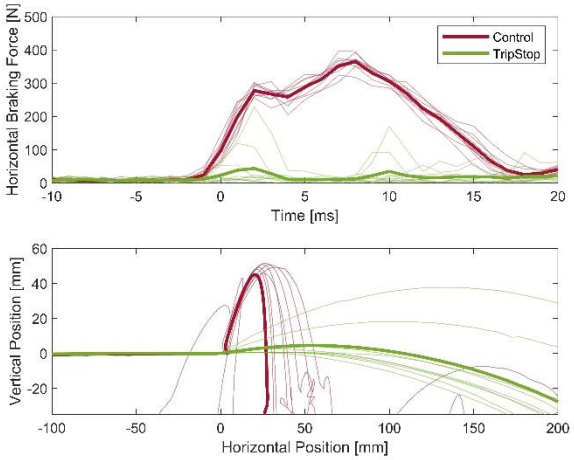

Figure. 2 Horizontal braking forces precented over time on the upper graph and vertical position of the shoe in vertical and horizontal axis on the lower graph. The control shoe is presented in red, and the safety shoe modified with TripStop in green. Each trial is presented by a thin line. The average of the 10 trials is presented with a thick line.

CONCLUSIONS

The friction and angle-modifying elements mounted on safety shoes lowered the peak horizontal braking force by 83% and the horizontal braking impulse by 85%. Furthermore, the modified shoe passed over the obstruction bar. This behavior of the modified shoe might be beneficial when recovering from a trip. Further, biomechanical tests are needed to verify trip recovery with the mounted TripStop.

ACKNOWLEDGEMENTS

This work was partly supported by the Danish Working Environment Research Fund (grant number 39-2021-09).

REFERENCES

1. Chang et al., Ergonomics, **59**:7, 861-883, 2016
2. Begg et al., Gait & Posture, **25**:191-198, 2007
3. Fong et al., Medicine & Science in Sports & Exercise, **37**: 0195-9131, 2005

AnyBody modeling driven by multi-modal data from wearable sensors

Mingyuan He[1,*], Shaoping Bai[1]
[1]Department of Materials and Production, Aalborg University, Denmark,
*Ph.D. student

INTRODUCTION

Nowadays, the applications of Human-Robot Collaboration (HRC) are widly used with the development of artificial intelligence. Thus, it is very important to build up human models to analyze the human motion. While IMU data is the most frequently used signals in obtaining movement information, bio-signals such as FMG can provide extra references for human intention. In this work, we developed a human model with multi-modal data collected by wearable sensors. An animation is generated to represent the real human motion, and further invastigations are carried out on joint displacements and muscle forces.

METHODS

We used the AAL sensor band from BIOX (Figure 1) as the wearable sensing device to detect human limb motion. The sensor band combines the FMG signals from Force Sensing Resistors (FSRs) with data from inertia measurement unit (IMU) [1]. In this experiment, there are two sensor bands located at upper-arm and forearm separately. The locations of sensor bands at the arms are not exactly required due to different biological sizes between people and inability to precisely fix the gap while wearing. However, the orientation of the sensor band is crucial for coordinating reference (Figure 2). Therefore, a base posture where the whole arm is naturally relaxed hanging is recorded before the motion begins.

Fig. 1 The AAL sensor band.

Fig. 2 Band mounting.

Samples are recorded while the subject performs various arm motions, such as waving, lifting, holding, laying down, and so on. The collected data along with the sampling time are processed in MATLAB. Filters are applied to remove the abnormal signals and decrease the noise. Then, the initial rotation matrices are calculated for both Humerus and Ulna based on IMU signals. For each iteration, the instant rotation matrix is multiplied by the initial rotation matrix and converted into Euler angles [2]. The rotation sequence of the Euler angles is consistent with the default setting of the AnyBody human model, which is the Abduction-Flexion-Rotation sequence. The results of Euler angles of each motion are rounded to 3 decimal digits and saved into file along with the sampling time.

The human model is generated from AnyBody standard template. For each of the five motions (Abduction, flexion and rotation for Humerus, flexion for Ulna, and pronation for Radius), a driver is assigned to ensure the joints rotate as the linked data. Instead of building and referring to a frame on the segments, the drivers are installed on the interfaces, which can control the defined motion more clearly. The interpolating drivers also enable AnyBody to render the animation coherently despite the uneven sampling time and different amounts of frames.

RESULTS AND DISCUSSION

Figure 3 demonstrates the frame that human model representing the real motion. Displacement of the joints and muscle forces can be studied [3] to comprehend the human action compared to IMU and FMG signals.

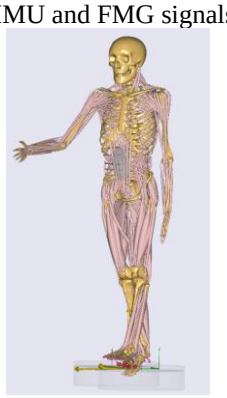

Fig. 3 Human model representing real motion.

CONCLUSIONS

In this work, we developed a human model in AnyBody, which is driven by multi-modal data collected from the wearable AAL sensor band. The generated animation is worthy in biomechanical analysis for further guidance on HRC.

REFERENCES

1. Muhammad AG, et al. *Modeling, Identification and Control*, **40**(4):189-198, 2019
2. Valenti RG, et al. *Sensors*, **15**(8):19302-19330, 2015
3. Michael Damsgaard, et al., *Simulation Modelling Practice and Theory* **14**(8): 1100-1111, 2006

Biomechanical Evaluation of Lumbar Interbody Fixation Techniques: A Comparative Study of Standalone Cages vs. 360-Fixation Constructs

Ali Kiapour[1], Mohammadjavad Einafshar[2*],Elie Massaad[1], John Shin[1]

1. Department of Neurosurgery, Massachusetts General Hospital, Harvard, Medical School, Boston, MA, USA.
2. Department of Material and Production, Aalborg University, Aalborg, Denmark.

INTRODUCTION

Low fusion rates and cage subsidence have been reported as the main drawbacks of lumbar fixation with static interbody cages [1]. Although several clinical and biomechanical studies have evaluated the efficacy of 360 interbody fixation constructs (Anterior cage plus posterior fixation) [2,3], no study has reported the biomechanical comparison between such constructs and more novel techniques which use standalone fixation implants [4]. A cadaver validated computational model of lumbar spine was used to compare the biomechanics of spine instrumented with 360 fixations versus standalone cage with screw and cage with lateral plate systems.

To compare the mechanical stability of different interbody fixation techniques in lumbar spinal segments with standalone interbody versus static cage with posterior fixation or lateral plate system.

METHODS

An experimentally validated Finite element (FE) model of L1-Pelvic segment (Figure 1) was used to simulate ALIF and LIF lumbar fixation techniques including: ALIF cage at L5-S1 plus posterior screw-rod fixation (360 construct) versus ALIF standalone (screw through the cage). LIF cage at L4-L5 versus LIF cage with integrated two-hole lateral plate system. 4WEB Medical's Truss ALIF (40mm x 28mm), Lateral Truss (26mm X 50mm) cages and 2-hole integrated plate systems were used for simulation of the surgical procedure. For 360 constructs, a generic posterior rod and screw system was used. All models were subjected to a 400N compressive pre-load followed by an 8 Nm moment to simulation Flexion-Extension, Left and Right Bending and Axial Rotation motions. The segmental kinematics and the load sharing at the inferior endplate were compared among the cases.

RESULTS

The segmental motion in standalone ALIF construct was 1.3°(Flex-Ext), 1.4° (LB) and 1° (AR) versus 1°, 1° and 0.7° in 360 ALIF in the same planes of motion. When comparing lateral constructs, the motions were 1.5° (Flex-Ext), 1.1° (LB) and 0.9° (AR) in Lateral cage with plate versus 1.1°, 1.0° and 0.8° in the 360-lateral construct for the same loads. The peak stresses in extension for the LIF stand-alone cage were slightly higher than the posterior instrumented cases. When comparing the mechanical stress on the inferior endplate of the index segment, the Stand-alone ALIF had almost 20% higher peak stress compared to the 360 ALIF construct. In the lateral construct, the cage-plate segment experienced 15% lower stresses on the endplate compared to the 360-lateral construct.

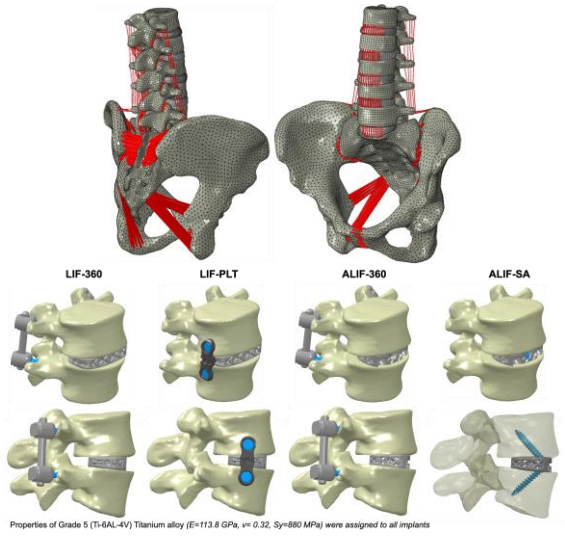

Figure 1: *a) Finite element model of lumbo-pelvic spine used in this study b) Lumbar spine motion segment instrumented with various interbody fixation constructs.*

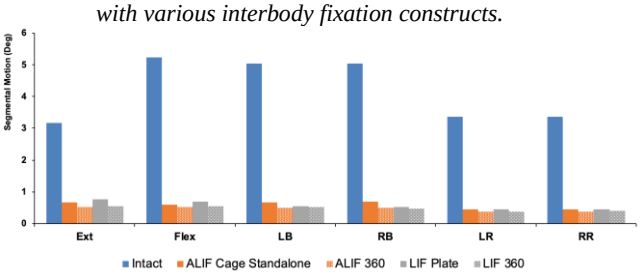

Figure 2: *Comparison of segmental range of motion among instrumented constructs versus intact.*

DISCUSSION

Our data suggest that the 360 construct were able to provide greater stability in the sagittal plane. The lateral cage with integrated plate had stability closed to the 360-lateral construct in axial rotation [1,2]. The standalone cage resulted in higher stresses at the endplate compared the 360 constructs. Standalone ALIF and LIF with lateral plate are biomechanically efficient alternatives to 360-fixation constructs at least under the controlled conditions analyzed in the present study. Clinical data are required to support the findings and defining the further role and application of stand-alone cages.

REFERENCES

[1] Kiapour, M et al. *J Spine*, **22(9)**: S17,2022.
[2] Kiapour, M et al. *J Neurosurg Spine*, **36(6)**: 928-936,2022.
[3] Einafshar, M et al. *J Arch Bone Jt Surg*, **10**: 204-212,2022.
[4] Einafshar, M. et al. *JOR spine*, **e1220**, *2022.*

Modulating Femoral Torsion: Evaluating the Impact of a Novel Plate Design in a Growing Porcine Model

Ahmed Haloum[1], Ole Rahbek[1], Søren Kold[1], Jan Rölfing[2], Shima Gholinezhad[1,3], John Rasmussen[3], Ahmed Abood[2]

[1]Department of Orthopaedic Surgery, Aalborg University Hospital, Denmark
[2]Department of Clinical Medicine - Orthopaedic surgery, Aarhus University, Denmark
[3]Department of Materials and Production, Aalborg University, Denmark

INTRODUCTION

While osteotomies remain essential for rotational correction and limb lengthening, less invasive methods can effectively address angular deformities or moderate length discrepancies. The evolution of epiphysiodesis techniques allows for gradual angular correction and/or length equalization through guided growth procedures, harnessing the body's innate growth potential for precise deformity corrections in children. Extensive efforts have been dedicated to refining plates tailored for guided growth surgery (1). In a prior feasibility study conducted within our research, we introduced an innovative z-shaped plate design (2). This distinctive z-shaped plate design incorporates two screws with bidirectional movement, allowing it to dynamically rotate in conjunction with natural bone growth. An important characteristic of this plate is its capacity to minimize the invasiveness of the surgical procedure, leading to reduced hospitalization durations. The evaluation of the plate's ability to induce femoral rotation and its precision yielded satisfactory results in a cadaverous in vitro study utilizing, with growth simulated via axial distraction of the osteotomy. Despite the promising outcomes, the plate's performance in the presence of natural growth remains unexplored. In this subsequent study, our objective was to assess the plate's functionality in the context of natural bone growth, utilizing a porcine model, in preparation for potential clinical application.

METHODS

To achieve this objective, we conducted experiments involving a cohort of 11 pigs, surgically implanting the novel plate on their left femur (ipsilateral), while their right femur served as a control (contralateral). During the surgical procedure, two plates were strategically positioned on both the lateral and medial sides of the distal femur, spanning the growth plate, with the intention of facilitating external rotation as longitudinal growth progressed.

To evaluate potential femoral rotation, a time-series of three-dimensional computed tomography (CT) scans was conducted, one immediately post-surgery (0-week bone) and another after a 12-week interval (12-week bone) to assess femoral torsion. Initially, we reconstructed 3D bone models using segmentation tools provided by the Mimics software. Then, we employed a 3D/3D surface registration approach (3) to align the two time points for each side and measure torsion in both the contralateral and ipsilateral femurs. While contralateral femoral torsion signified the effects of normal growth, the measurement in the ipsilateral femur encompassed both the influence of natural growth and the surgical intervention. Examining the disparity between these measurements allowed us to specifically determine the impact of the intervention.

RESULTS AND DISCUSSION

The surgical intervention led to a significant disparity in the rotation rates between the ipsilateral and contralateral femurs ($p<0.05$). Specifically, the surgery induced lateral rotation (-3.97±3.81) along the axial axis of the ipsilateral femur, while the contralateral femur, exhibited a slight medial rotation (2.81±2.00). The intervention also resulted in rotational changes along the coronal axis, leading to alterations in condyle shape. These changes included an outward rotation of the condyles (valgus) or an inward rotation and compression of the condylar surface (varus). We also observed minimal impact around the sagittal axis, with limited significant morphological alterations observed in this study.

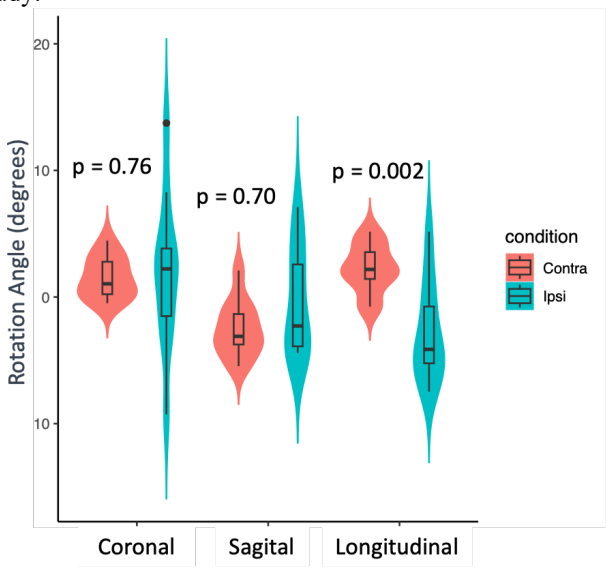

Fig. 1. An overview of the study results.

This study provides promising results concerning the plate's effectiveness in femoral rotation when applied to a growing animal model. This work serves as a crucial initial step in validating the technique and identifying potential side effects before advancing to future clinical investigations.

Further data analysis, particularly focused on adverse effects like limb length disparities, angular and joint deformities, and rebound effects, is currently underway.

REFERENCES

1. Eastwood, D. M., and A. P. Sanghrajka. "Guided growth: recent advances in a deep-rooted concept", The Journal of Bone & Joint Surgery, (2011).
2. Abood, Ahmed A., et al. "Controlled rotation of long bones by guided growth: A proof of concept study of a novel plate in cadavers", Journal of Orthopaedic Research, (2022).
3. Audette, Michel Aet al. "An algorithmic overview of surface registration techniques for medical imaging." Medical image analysis, (2000)

Quest for Accuracy: Progressing Towards Optimal Ultrasound Settings for Bone-Soft Tissue Interface Identification

Martin Vorup Lindvand[1,*], Nico Verdonschot[2], Ilias Theodorakos[1], and Michael S. Andersen[1]

[1]Aalborg University, Departmend of Materials and Production

[2] Nijmegen University

*Ph.D. student

INTRODUCTION

Accurate bone movement tracking under varying loads is vital for determining bone kinematics, which must be precise to within 1 degree or 1 mm for clinical applications [1]. However, conventional methods rely on costly, invasive, and limited-field-of-view medical imaging such as X-ray imaging which restricts the clinical usage. An alternative, non-invasive approach is an ultrasound-based system for comprehensive 3D joint kinematics quantification.

Recent research by Niu et al. showcased the viability of using A-mode ultrasound probes for knee joint kinematics recording, achieving a maximum RMSE of 3.44 degrees for rotations and 4.88 mm for translations using 30 probes [2]. However, utilizing A-mode probes poses challenges in accurately distinguishing bone peaks amid amplitude peaks influenced by intricate soft tissue interactions [3,4].

This investigation focuses on the impact of varied ultrasound transmission settings on bone peak detection, intending to optimize the non-invasive utility of ultrasound in joint kinematics assessment.

METHODS

A 7.5 MHz dual-element A-mode probe was used to evaluate ultrasound settings from Table 1, facilitated by the Verasonics Vantage 32LE System.

The study involved a cadaveric lower limb specimen, thawed a day before the experiment, and initiated with the probe placed at the femoral trochanter major following palpation.

The arrangement was located within a CT scanner to obtain images for ascertaining the true distance between the probe and the bone surface, derived from segmented CT images. The experimental data analysis procedure consists of:

Identifying and graphing peaks that matched specific characteristics from previous experiments based on peak width and prominence.

Choosing the presumed bone peak.

Conducting a comparison with the ground truth distance.

RESULTS AND DISCUSSION

Among the peaks for every setting meeting the width, amplitude, and prominence criteria values, one was selected based on the comprehensive pattern of the received data and then compared to the ground truth of 9.81 mm. The results can be seen in Table 2.

Table 1 – peak distances for some of the settings in mm.

The peak selection hinges on data shape and curvature. The optimal bone peak is envisioned as sharp, with high amplitude, devoid of local minima, and showing minimal signal trailing due to the bone's pronounced attenuation. Nonetheless, the interaction of bone with sound may induce blurring, attributed to the reverberation phenomenon involving strong parallel reflectors.

REFERENCES

[1] Dennis, D. A., Mahfouz, M. R., Komistek, R. D., and Hoff, W., 2005, J. Biomech., 38(2)

[2] Niu, K., Sluiter, V., Sprengers, A., Homminga, J., and Verdonschot, N., 2017

[3] Scheipers, U., Ermert, H., Sommerfeld, H.-J., Garcia-Schürmann, M., Senge, T., and Philippou, S., 2003, Ultrasound Med. Biol., 29(8)

[4] Schmitz, G., Ermert, H., and Senge, T., 1999, IEEE Trans. Ultrason. Ferroelectr. Freq. Control, 46(1)

Table 1 - Ultrasound transmission settings tested

Setting	Test 1	Test 2	Test 3
Transmission voltage	70	80	90
Spatial Pulse Length	2	4	6
Time-Gain Compensation	[0, 136, 271, 407, 543, 679, 814, 950]	[100, 221, 343, 464, 586, 707, 829, 950]	[200, 307, 414, 521, 629, 739, 843, 950]

Table 2 - peak distances for some of the settings in mm.

	TGC-1	TGC-2	TGC-3	SPL-6	SPL-4	SPL-2
US Distance	9.7	11.9	13.7	10.1	9.6	9.5
Difference	0.11	2.09	3.89	0.29	0.21	0.31

Sensitivity Analysis of Cartilage Creep Material Properties Prediction in Unconfined Compression: Impact of Data Quantity

Bo E. Seiferheld[1*] and Michael S. Andersen[1]
[1]Department of Materials and Production, Aalborg University, Denmark
*Ph.D. student. bes@mp.aau.dk

INTRODUCTION

Osteoarthritis (OA), a prevalent and debilitating disease, involves progressive cartilage loss and altered joint features [1]. This has pushed advancements in cartilage tissue engineering for treatment and healing. Mechanical testing is crucial in the evaluation, but inconsistent testing techniques, across studies, leads to data misinterpretation and impede meaningful comparisons [2]. A recent review emphasized the need for 1 MPa creep stress with >60-min relaxation. Therefore, this study aims to assess the impact of data quantity on cartilage creep material property predictions, offering guidance for creep testing time modes.

METHODS

Ex vivo unconfined compression creep experiments were conducted using cylindrical 6-mm diameter, full-thickness cartilage samples (n = 11) extracted from bovine knees. An Instron material testing machine (Model 5944) performed creep experiments in a force-controlled setting with a preload of 0.05 MPa. After 15 minutes of preload, to reach baseline thickness and even out irregularities [3], a force ramping rate of 0.25 MPa/s reached the creep load of 1 MPa within 4 seconds. Creep load was maintained for 5 hours with continuous force and displacement recording at 10 Hz.

Experimental creep strain was split into six-time intervals (30, 60, 120, 180, 240 and 300 minutes) and fitted to two different models: (1) a standard linear solid model in Kelvin form and (2) a standard linear solid model with the elastic modulus (E_1) constrained and directly determined from the raw data. The creep equation [4] is as follows:

$$\varepsilon(t) = \frac{\sigma_0}{E_1} + \frac{\sigma_0}{E_2}\left(1 - e^{\left(-\frac{t}{\tau}\right)}\right) \quad (1)$$

where ε is creep strain at time t, under constant stress, σ_0. E_1 is the initial elastic modulus, E_2 is the steady state elastic modulus and τ is the time constant for equilibrium. MATLAB 2022b was used for a nonlinear least-squares curve-fitting.

RESULTS AND DISCUSSION

The samples exhibited a baseline thickness of 2.06 ± 0.56 mm and reached a mean strain of 0.59 ± 0.06 at creep equilibrium. The initial strain following the ramp-up to the creep load averaged 0.14 ± 0.06, with an associated elastic modulus of 7.12 ± 2.62 MPa. All samples reached a well-defined equilibrium, as evidenced by less than 0.6 microns of deformation over one minute, achieved after 124 ± 23 minutes of loading, with a corresponding strain of 0.56 ± 0.06, only 5% deviating from the final creep strain.

The results highlight a noteworthy observation: Model 1 tends to gradually overestimate E_1 with optimiser bias toward fitting the viscous component, ultimately improving model fit. However, this inclination brings the solution closer to E_2 and τ. Conversely, Model 2 exhibits a fitting bias towards the linear elastic region, resulting in an underestimation of the viscous properties.

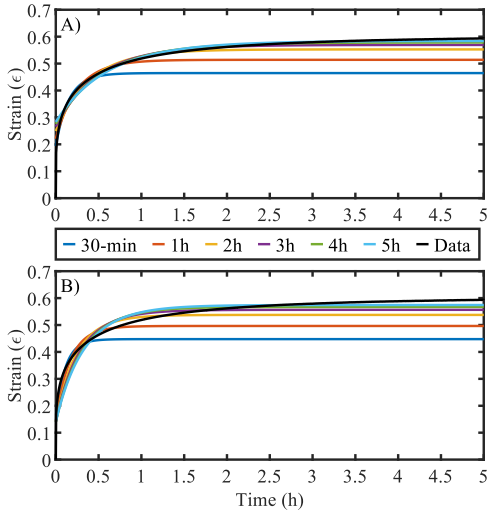

Fig. 1 Predicted strain based on six different time intervals with model 1 (A) and model 2 (B) and corresponding ground truth data in black.

CONCLUSIONS

For unconfined creep testing, it is advisable to maintain the stress for at least 2 hours to acquire sufficient information for model fitting. Lastly, setting a clear criterion for defining equilibrium and enrolling only those samples that meet this criterion are recommended.

REFERENCES

1. Glyn-Jones et al. *The Lancet* **386**: 376-387, 2015.
2. Patel et al. *Tissue Eng Part C Methods* **25**: 593-608, 2019.
3. Athanasiou et al. *J. Ortho Res* **9**: 330-340, 1991.
4. Gong et al. *J. Healthc Eng* **2019**: 1-9, 2019.

Table 1 Cartilage material properties at different time intervals with the corresponding R^2 values.

	Model 1				Model 2		
	E_1 (MPa)	E_2 (MPa)	τ (sec)	R^2	E_2 (MPa)	τ (sec)	R^2
30-min	5.64 ± 1.59	3.75 ± 0.47	565 ± 87	0.72 ± 0.08	3.31 ± 0.40	395 ± 73	0.62 ± 0.08
60-min	4.87 ± 1.26	3.46 ± 0.39	943 ± 124	0.86 ± 0.05	2.85 ± 0.31	614 ± 112	0.75 ± 0.07
120-min	4.25 ± 0.99	3.33 ± 0.35	1464 ± 226	0.94 ± 0.02	2.55 ± 0.27	892 ± 168	0.85 ± 0.05
180-min	3.97 ± 0.86	3.32 ± 0.34	1818 ± 338	0.96 ± 0.01	2.43 ± 0.26	1066 ± 214	0.89 ± 0.04
240-min	3.80 ± 0.79	3.34 ± 0.33	2075 ± 429	0.97 ± 0.01	2.37 ± 0.26	1184 ± 251	0.91 ± 0.04
300-min	3.69 ± 0.75	3.35 ± 0.32	2265 ± 500	0.97 ± 0.01	2.33 ± 0.27	1268 ± 279	0.92 ± 0.03

ROBOT-ASSISTED WEIGHT RELIEF FOR PREVENTION OF MUSCULOSKELETAL PAIN AMONG BRONCHOSCOPISTS

Knudsen PK[1,2], Jepsen RB[1], Sørensen AS[1], Juul AD[2], Andersen JF[1], Deleuran MK[2], Dalager T[1], Søgaard K[1]

[1]Syddansk Universitet, [2]Odense Universitetshospital

INTRODUCTION

Musculoskeletal disorders (MSDs) are a common challenge among endoscopists due to prolonged awkward postures during procedures [1]. A study involving clinicians performning pulmonary endoscopic procedures, specifially bronchoscopists, revealed that 50.6% of survey respondents reported musculoskeletal pain [2]. Among endoscopists, the most severe regions of pain reported are the back, neck, and shoulders [2**,** 3]. This study investigated the effects of a robotic weight relief system for alleviating the physician's arm during simulated bronchoscopy to reduce MSDs.

METHODS

Six experienced bronchoscopists from the Department of Respiratory Medicine at Odense University Hospital participated in the study using a repeated-measures design. They each conducted two 40-minutes bronchoscopies on a GI-BRONCH Mentor endoscopy simulator, one conventional procedure and one using the robotic weight relief system, which was attached to the arm holding the bronchoscope. Bipolar surface electromyography (EMG) recordings were collected from the forearm, shoulder, neck extensors, and upper trapezius, and an Amplitude Probability Distribution Function (APDF) was calculated to find the static, median, and peak levels of muscle activity. Changes in arm movement patterns were investigated using accelerometer data. Subjective assessments were made using the Borg CR10 scale for perceived exertion and the System Usability Scale (SUS) to evaluate the usability of the system.

RESULTS AND DISCUSSION

The APDF indicated increased forearm muscle activity during the weight-relieved bronchoscopy compared to the conventional procedure (Table 1). This increase in muscle activity was likely due to the attachment of the robotic system to the wrist, requiring the subject to make ulnar deviation to maintain a stable and vertical position of the scope. For the shoulder, the APDF showed reduced muscle activity when performing the weight-relieved bronchoscopy, with statistical significance observed for the peak level for anterior deltoid and the static level for medial deltoid (Table 1). No considerable changes were observed for the neck extensors and upper trapezius muscles. Overall, the EMG analysis indicated that the robotic system was more demanding on the forearm and less demanding on the shoulder compared to the conventional procedure.

The study found an average increase in arm elevation angle of 5.9 degrees during the weight-relieved bronchoscopy. The increase in arm elevation angle along with the decrease in shoulder muscle activity suggests that the robotic system may be effective in preventing MSDs in procedures that require elevated arm positions and allow for better flexibility and variation without increasing the shoulder load. Additionally, the perceived exertion was lower during the weight-relieved bronchoscopy (1.9 vs. 2.4), and the usability of the system was assessed to be above average with a SUS score of 73.3.

CONCLUSIONS

While the EMG analysis did not unambiguously demonstrate the effectiveness of the weight-relieved bronchoscopy over the conventional procedure, the subjective measures and the changes in arm movement pattern indicated a positive impact of the robotic system. This provides an incentive for further development of the system to improve its effectiveness in reducing musculoskeletal pain among bronchoscopists.

REFERENCES

1. Kamani L, Kalwar H, *Clin Endosc* **54(3)**: 356-362, 2021
2. Gilbert CR, et al., *J Bronchology Interv Pulmonol* **20(2)**: 113-20, 2013
3. Yung DE, et al., *Expert Rev Gastroenterol Hepatol* **11(10)**: 939-947, 2017

Table 1 Median values for the Amplitude Probability Distribution Function for each muscle (expressed in %EMGmax) for the static level (10), median level (50), and peak level (90). Wilcoxon signed-rank analysis is used and the P-value is provided. Statistical significance is indicated by a * with α=0.05.

	Median APDF values (expressed in %EMGmax)		
	With robotic weight relief 10 (50) 90	**Without robotic weight relief 10 (50) 90**	**P-value (*) 10 (50) 90**
Extensor carpi radialis	5.1 (10.1) 15.3	4.5 (8.4) 14.3	0.69 (0.44) 1.00
Extensor carpi ulnaris	3.1 (8.0) 20.4	2.7 (7.2) 22.6	0.31 (1.00) 0.06
Flexor digitorium superficialis	1.7 (5.1) 10.5	2.2 (5.0) 10.3	0.06 (0.44) 1.00
Anterior deltoid	1.6 (4.2) 6.5	2.1 (5.5) 8.3	0.31 (0.31) 0.03*
Medial deltoid	0.9 (1.1) 1.6	1.1 (1.3) 1.8	0.03* (0.06) 0.31

CLASSIFICATION OF JAW MOVEMENTS FROM TMD PATIENTS BASED ON PCA

Ryuji Shigemitsu[1,2,*], Takehiko Mito[1], Emika Sato[1], Hiroshi Egusa[1], Keiichi Sasaki[1] and John Rasmussen[2]

[1] Division of Advanced Prosthetic Dentistry, Tohoku University Graduate School of Dentistry, Sendai 980-8575, Japan
[2] Department of Materials and Production, Aalborg University, Fibigerstrade 16, Aalborg East DK-9220, Denmark

INTRODUCTION

Temporomandibular disorders (TMD) are regarded as the third most common dental disease. TMD is characterized by symptoms such as temporomandibular joint noises, pain, and impaired jaw movements. Thus, jaw movement recording is a common assessment method during the TMD treatment process. This study aims to classify time-series jaw movement data obtained during the treatment process of TMD using principal component analysis (PCA) and Cluster analysis. This will enable dentists to visualize the changes in jaw movement based on the progression of TMD treatment.

METHODS

This study was conducted with the approval of the Ethics Committee of Tohoku University Graduate School of Dentistry (No: 33541). A total of eight subjects (five symptomatic TMD patients and three asymptomatic subjects) participated in this study. TMD patients with impairment of jaw movement were referred to appliance therapy and physical therapy for dental treatment. At several time points during their treatment process, the maximum unassisted opening-closing movements were recorded by an orthodontic motion capture system (ARCUS digma Ⅱ, Kavo, Germany). In total, the data set comprises 25 trials. The jaw motion data were transferred to the AnyBody Modeling System [1] (AnyBody Technology, Aalborg, Denmark) and used to drive a musculoskeletal model from which joint angle time series were extracted and transformed into Fourier series for compact and consistent representation. The coefficients were subjected to principal component analysis (PCA), and subsequently to cluster analysis (k-means) to classify the jaw movements at each time point in the treatment into two clusters. The treatment progress was then observed on a map of the two dominant principal components.

RESULTS AND DISCUSSION

Fig.1 reveals that motion variation over the course of the treatment is indeed dominated by some variables over others, but the two first principal components describe only about 28% of the variance.

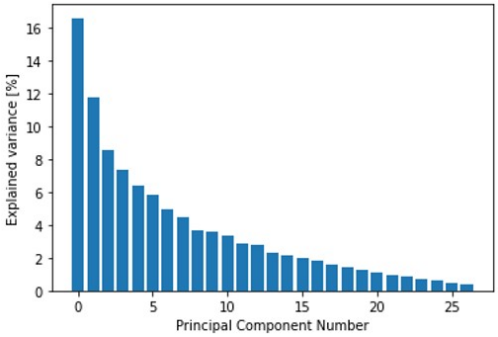

Fig. 1 Histogram of the explained variance of each principal component.

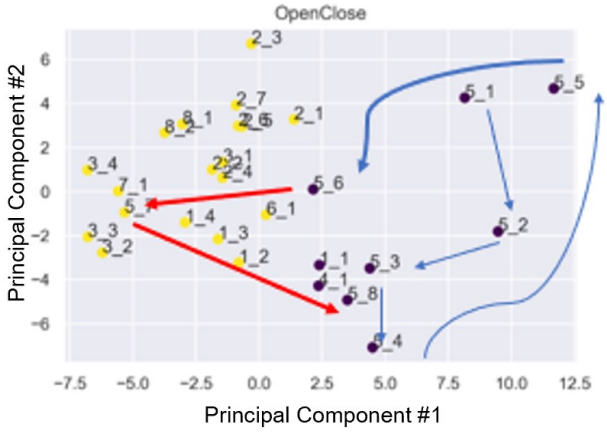

Fig. 2 Cluster analysis in the space of the two dominating principal components. Patient 5 initially dominates the second cluster but is returned to the first cluster during the treatment.

Despite the small data set, the results indicate that it may be possible to classify TMJ patients and the treatment effect objectively from motion capture data (Fig.2). The treatment pathway of subject no. 5 with symptoms leads from the "symptomatic" cluster to the asymptomatic cluster in accordance with the improvement of the clinical symptoms over the treatment progress. The authors previously reported on the setting of boundary conditions for the patient-specific bony surfaces for individual patients in musculoskeletal analysis [2]. These studies show promise for a novel functional assessment for TMD patients based on the kinematic features.

CONCLUSIONS

It may be possible to objectively classify movement data from TMD patients into symptomatic and asymptomatic clusters, but larger data sets are required for a definite conclusion.

ACKNOWLEDGEMENTS

This work was supported by JSPS KAKENHI Grant Number 21KK0292.

REFERENCES

1. Damsgaard M,et al. Analysis of musculoskeletal systems in the AnyBody Modeling System. *Simulation Modelling Practice and Theory*. **14**(8):1100-11, 2006
2. Shigemitsu R, et al.. Musculoskeletal Modeling with Jaw Motion Data from a TMD Patient. *Advances in Transdisciplinary Engineering*. **11**:118-4, 2020